JHEP

Published for SISSA by Springer

Received: July 23, 2013
Accepted: August 30, 2013
Published: September 25, 2013

Measurements of branching fractions of leptonic and hadronic D_s^+ meson decays and extraction of the D_s^+ meson decay constant

The BELLE collaboration

A. Zupanc,[w] I. Adachi,[m] H. Aihara,[bf] K. Arinstein,[c] D.M. Asner,[as] T. Aushev,[t] A.M. Bakich,[az] A. Bala,[at] B. Bhuyan,[o] G. Bonvicini,[bl] A. Bozek,[ao] M. Bračko,[ad,u] J. Brodzicka,[ao] T.E. Browder,[l] M.-C. Chang,[h] P. Chang,[an] V. Chekelian,[ae] A. Chen,[al] P. Chen,[an] B.G. Cheon,[k] K. Chilikin,[t] R. Chistov,[t] K. Cho,[x] V. Chobanova,[ae] S.-K. Choi,[j] Y. Choi,[ay] D. Cinabro,[bl] J. Dalseno,[ae,bb] M. Danilov,[t,ag] Z. Doležal,[d] Z. Drásal,[d] D. Dutta,[o] S. Eidelman,[c] H. Farhat,[bl] J.E. Fast,[as] T. Ferber,[g] V. Gaur,[ba] N. Gabyshev,[c] S. Ganguly,[bl] R. Gillard,[bl] Y.M. Goh,[k] B. Golob,[ab,u] J. Haba,[m] T. Hara,[m] K. Hayasaka,[aj] H. Hayashii,[ak] Y. Horii,[aj] Y. Hoshi,[bd] W.-S. Hou,[an] Y.B. Hsiung,[an] H.J. Hyun,[z] T. Iijima,[aj,ai] K. Inami,[ai] A. Ishikawa,[be] R. Itoh,[m] Y. Iwasaki,[m] T. Iwashita,[ak] I. Jaegle,[l] T. Julius,[af] E. Kato,[be] H. Kawai,[e] T. Kawasaki,[aq] H. Kichimi,[m] C. Kiesling,[ae] D.Y. Kim,[ax] H.O. Kim,[z] J.B. Kim,[y] J.H. Kim,[x] M.J. Kim,[z] Y.J. Kim,[x] K. Kinoshita,[f] J. Klucar,[u] B.R. Ko,[y] P. Kodyš,[d] S. Korpar,[ad,u] P. Križan,[ab,u] P. Krokovny,[c] B. Kronenbitter,[w] T. Kuhr,[w] T. Kumita,[bh] A. Kuzmin,[c] Y.-J. Kwon,[bn] J.S. Lange,[i] S.-H. Lee,[y] J. Li,[aw] J. Libby,[o] Z. Q. Liu,[p] D. Liventsev,[m] P. Lukin,[c] H. Miyata,[aq] R. Mizuk,[t,ag] G.B. Mohanty,[ba] A. Moll,[ae,bb] R. Mussa,[s] E. Nakano,[ar] M. Nakao,[m] E. Nedelkovska,[ae] N. K. Nisar,[ba] S. Nishida,[m] O. Nitoh,[bi] S. Ogawa,[bc] S. Okuno,[v] G. Pakhlova,[t] C.W. Park,[ay] H. Park,[z] H.K. Park,[z] T.K. Pedlar,[ac] R. Pestotnik,[u] M. Petrič,[u] L.E. Piilonen,[bk] M. Prim,[w] M. Ritter,[ae] M. Röhrken,[w] A. Rostomyan,[g] S. Ryu,[aw] H. Sahoo,[l] T. Saito,[be] Y. Sakai,[m] S. Sandilya,[ba] L. Santelj,[u] T. Sanuki,[be] Y. Sato,[be] V. Savinov,[au] O. Schneider,[aa] G. Schnell,[a,n] C. Schwanda,[r] A.J. Schwartz,[f] D. Semmler,[i] K. Senyo,[bm] M.E. Sevior,[af] M. Shapkin,[q] C.P. Shen,[b] T.-A. Shibata,[bg] J.-G. Shiu,[an] B. Shwartz,[c] A. Sibidanov,[az] F. Simon,[ae,bb] Y.-S. Sohn,[bn] A. Sokolov,[q] E. Solovieva,[t] M. Starič,[u] M. Steder,[g] T. Sumiyoshi,[bh] U. Tamponi,[s,bj] K. Tanida,[aw] G. Tatishvili,[as]

Open Access

doi:10.1007/JHEP09(2013)139

JHEP09(2013)139

Y. Teramoto,[ar] **K. Trabelsi,**[m] **T. Tsuboyama,**[m] **M. Uchida,**[bg] **T. Uglov,**[t,ah] **S. Uno,**[m] **Y. Usov,**[c] **S.E. Vahsen,**[l] **C. Van Hulse,**[a] **P. Vanhoefer,**[ae] **G. Varner,**[l] **A. Vinokurova,**[c] **V. Vorobyev,**[c] **M.N. Wagner,**[i] **C.H. Wang,**[am] **M.-Z. Wang,**[an] **P. Wang,**[p] **X.L. Wang,**[bk] **M. Watanabe,**[aq] **Y. Watanabe,**[v] **E. Won,**[y] **Y. Yamashita,**[ap] **S. Yashchenko,**[g] **Z.P. Zhang,**[av] **V. Zhilich**[c] **and V. Zhulanov**[c]

[a] *University of the Basque Country UPV/EHU, 48080 Bilbao, Spain*
[b] *Beihang University, Beijing 100191, PR China*
[c] *Budker Institute of Nuclear Physics SB RAS and Novosibirsk State University, Novosibirsk 630090, Russian Federation*
[d] *Faculty of Mathematics and Physics, Charles University, 121 16 Prague, The Czech Republic*
[e] *Chiba University, Chiba 263-8522, Japan*
[f] *University of Cincinnati, Cincinnati, OH 45221, U.S.A.*
[g] *Deutsches Elektronen–Synchrotron, 22607 Hamburg, Germany*
[h] *Department of Physics, Fu Jen Catholic University, Taipei 24205, Taiwan*
[i] *Justus-Liebig-Universität Gießen, 35392 Gießen, Germany*
[j] *Gyeongsang National University, Chinju 660-701, South Korea*
[k] *Hanyang University, Seoul 133-791, South Korea*
[l] *University of Hawaii, Honolulu, HI 96822, U.S.A.*
[m] *High Energy Accelerator Research Organization (KEK), Tsukuba 305-0801, Japan*
[n] *Ikerbasque, 48011 Bilbao, Spain*
[o] *Indian Institute of Technology Guwahati, Assam 781039, India*
[p] *Institute of High Energy Physics, Chinese Academy of Sciences, Beijing 100049, PR China*
[q] *Institute for High Energy Physics, Protvino 142281, Russian Federation*
[r] *Institute of High Energy Physics, Vienna 1050, Austria*
[s] *INFN — Sezione di Torino, 10125 Torino, Italy*
[t] *Institute for Theoretical and Experimental Physics, Moscow 117218, Russian Federation*
[u] *J. Stefan Institute, 1000 Ljubljana, Slovenia*
[v] *Kanagawa University, Yokohama 221-8686, Japan*
[w] *Institut für Experimentelle Kernphysik, Karlsruher Institut für Technologie, 76131 Karlsruhe, Germany*
[x] *Korea Institute of Science and Technology Information, Daejeon 305-806, South Korea*
[y] *Korea University, Seoul 136-713, South Korea*
[z] *Kyungpook National University, Daegu 702-701, South Korea*
[aa] *École Polytechnique Fédérale de Lausanne (EPFL), Lausanne 1015, Switzerland*
[ab] *Faculty of Mathematics and Physics, University of Ljubljana, 1000 Ljubljana, Slovenia*
[ac] *Luther College, Decorah, IA 52101, U.S.A.*
[ad] *University of Maribor, 2000 Maribor, Slovenia*
[ae] *Max-Planck-Institut für Physik, 80805 München, Germany*
[af] *School of Physics, University of Melbourne, Victoria 3010, Australia*
[ag] *Moscow Physical Engineering Institute, Moscow 115409, Russian Federation*
[ah] *Moscow Institute of Physics and Technology, Moscow Region 141700, Russian Federation*
[ai] *Graduate School of Science, Nagoya University, Nagoya 464-8602, Japan*
[aj] *Kobayashi-Maskawa Institute, Nagoya University, Nagoya 464-8602, Japan*
[ak] *Nara Women's University, Nara 630-8506, Japan*

JHEP09(2013)139

[al] National Central University, Chung-li 32054, Taiwan
[am] National United University, Miao Li 36003, Taiwan
[an] Department of Physics, National Taiwan University, Taipei 10617, Taiwan
[ao] H. Niewodniczanski Institute of Nuclear Physics, Krakow 31-342, Poland
[ap] Nippon Dental University, Niigata 951-8580, Japan
[aq] Niigata University, Niigata 950-2181, Japan
[ar] Osaka City University, Osaka 558-8585, Japan
[as] Pacific Northwest National Laboratory, Richland, WA 99352, U.S.A.
[at] Panjab University, Chandigarh 160014, India
[au] University of Pittsburgh, Pittsburgh, PA 15260, U.S.A.
[av] University of Science and Technology of China, Hefei 230026, PR China
[aw] Seoul National University, Seoul 151-742, South Korea
[ax] Soongsil University, Seoul 156-743, South Korea
[ay] Sungkyunkwan University, Suwon 440-746, South Korea
[az] School of Physics, University of Sydney, NSW 2006, Australia
[ba] Tata Institute of Fundamental Research, Mumbai 400005, India
[bb] Excellence Cluster Universe, Technische Universität München, 85748 Garching, Germany
[bc] Toho University, Funabashi 274-8510, Japan
[bd] Tohoku Gakuin University, Tagajo 985-8537, Japan
[be] Tohoku University, Sendai 980-8578, Japan
[bf] Department of Physics, University of Tokyo, Tokyo 113-0033, Japan
[bg] Tokyo Institute of Technology, Tokyo 152-8550, Japan
[bh] Tokyo Metropolitan University, Tokyo 192-0397, Japan
[bi] Tokyo University of Agriculture and Technology, Tokyo 184-8588, Japan
[bj] University of Torino, 10124 Torino, Italy
[bk] CNP, Virginia Polytechnic Institute and State University, Blacksburg, VA 24061, U.S.A.
[bl] Wayne State University, Detroit, MI 48202, U.S.A.
[bm] Yamagata University, Yamagata 990-8560, Japan
[bn] Yonsei University, Seoul 120-749, South Korea

E-mail: anze.zupanc@ijs.si

JHEP09(2013)139

Abstract: We present measurements of absolute branching fractions of hadronic and leptonic D_s^+ decays to $K^-K^+\pi^+$, $\overline{K}^0K^+$, $\eta\pi^+$, $\mu^+\nu_\mu$ and $\tau^+\nu_\tau$ and report a search for the leptonic $D_s^+ \to e^+\nu_e$ decays. The results are obtained from a data sample of 913 fb^{-1} collected at or near the $\Upsilon(4S)$ and $\Upsilon(5S)$ resonances with the Belle detector at the KEKB asymmetric-energy e^+e^- collider. The branching fractions of hadronic decays are measured to be

$$\begin{aligned}\mathcal{B}(D_s^+ \to K^-K^+\pi^+) &= (5.06 \pm 0.15 \pm 0.21)\%,\\ \mathcal{B}(D_s^+ \to \overline{K}^0K^+) &= (2.95 \pm 0.11 \pm 0.09)\%,\\ \mathcal{B}(D_s^+ \to \eta\pi^+) &= (1.82 \pm 0.14 \pm 0.07)\%,\end{aligned}$$

where the first and second uncertainties are statistical and systematic, respectively. The branching fractions of leptonic decays are measured to be

$$\begin{aligned}\mathcal{B}(D_s^+ \to \mu^+\nu_\mu) &= (0.531 \pm 0.028 \pm 0.020)\%,\\ \mathcal{B}(D_s^+ \to \tau^+\nu_\tau) &= (5.70 \pm 0.21^{+0.31}_{-0.30})\%,\end{aligned}$$

which are combined to determine the D_s^+ meson decay constant

$$f_{D_s} = (255.5 \pm 4.2 \pm 5.1)\ \text{MeV}.$$

We find no significant signal for $D_s^+ \to e^+\nu_e$ decays and set an upper limit of $\mathcal{B}(D_s^+ \to e^+\nu_e) < 1.0(0.83) \times 10^{-4}$ at 95% (90%) confidence level.

Keywords: e+-e- Experiments, Charm physics, Branching fraction, Flavor physics, Rare decay

ArXiv ePrint: 1307.6240

JHEP09(2013)139

Contents

JHEP09(2013)139

1 Introduction

Precise determination of the Cabibbo-Kobayashi-Maskawa (CKM) quark mixing matrix leads to a deeper understanding of the flavor structure in the Standard Model (SM) and provides a portal to New Physics (NP) processes at higher energy scales. Many of the constraints on the CKM unitarity triangle given by the precise experimental results on decays of B mesons (see ref. [1] for a review of results from the Belle collaboration) rely on lattice gauge theory (LQCD) calculations of quantities that parameterize nonperturbative QCD contributions to weak decays and mixing (see section 17 in ref. [2] for a review). Among these quantities, the pseudoscalar meson decay constants play an important role — without them, for example, an interpretation of measurements of purely leptonic decays $B^+ \to \tau^+ \nu_\tau$ [3, 4] and $B_s^0 \to \mu^+ \mu^-$ [5] that are particularly sensitive to NP contributions is

not possible. In some NP scenarios, the leptonic decay rates of the D_s^+ mesons could also be modified although the expected effects are smaller than in the B meson sector [6–9]. Measurements of leptonic decays of charmed hadrons, $D_s^+ \to \ell^+\nu_\ell$ where $\ell^+ = e^+$, μ^+ or τ^+, therefore enable precision tests of LQCD calculations of decay constants performed in the charm sector and can provide additional constraints on NP.[1]

Purely leptonic decays of mesons are among the simplest and theoretically cleanest processes. The branching fraction of D_s^+ meson leptonic decays that proceed via the mutual annihilation of the c and $\overline{s}$-quarks into a virtual W^+ boson is given in the SM by

$$\mathcal{B}(D_s^+ \to \ell^+\nu_\ell) = \frac{\tau_{D_s} m_{D_s}}{8\pi} f_{D_s}^2 G_F^2 |V_{cs}|^2 m_\ell^2 \left(1 - \frac{m_\ell^2}{m_{D_s}^2}\right)^2 . \tag{1.1}$$

Here, m_{D_s} is the D_s^+ meson mass, τ_{D_s} is its lifetime, m_ℓ is the lepton mass, V_{cs} is the relevant CKM matrix element, and G_F is the Fermi coupling constant. The parameter f_{D_s} is the D_s^+ meson decay constant and is related to the wave-function overlap of the meson's constituent quark and anti-quark. The leptonic decays of pseudoscalar mesons are suppressed by helicity conservation and their decay rates are thus proportional to the square of the charged lepton mass. Leptonic D_s^+ decays into electrons with $\mathcal{B} \sim 10^{-7}$ are not observable yet whereas decays to taus are favored over decays to muons. In particular, the ratio of the latter decays is equal to $R_{\tau/\mu}^{D_s} \equiv \mathcal{B}(D_s^+ \to \tau^+\nu_\tau)/\mathcal{B}(D_s^+ \to \mu^+\nu_\mu) = m_\tau^2/m_\mu^2 \cdot (1-m_\tau^2/m_{D_s}^2)^2/(1-m_\mu^2/m_{D_s}^2)^2 = 9.762 \pm 0.031$, based on the world average masses of the muon, tau and D_s^+ meson given in ref. [2]. Any deviation from this expectation could only be interpreted as violation of lepton universality in charged currents and would hence point to NP effects [10].

In the context of the SM, a measurement of $\mathcal{B}(D_s^+ \to \ell^+\nu_\ell)$ determines the D_s^+ meson decay constant since the magnitude of the CKM matrix element $|V_{cs}|$ is precisely determined from other measurements and the assumption that the CKM matrix is unitary. Measurements of f_{D_s} have been made previously by several groups: CLEO [11–13], Belle [14] and BaBar [15]. The current world average is $f_{D_s}^{\rm exp} = (260.0 \pm 5.4)$ MeV [2]. Within the SM, f_{D_s} has been predicted using several methods [16–23] and most calculations give values lower than the f_{D_s} measurement although within theoretical and experimental uncertainties. The largest discrepancy is with an unquenched LQCD calculation that yields $f_{D_s}^{\rm LQCD} = (248.0 \pm 2.5)$ MeV [16]. Measurements of f_{D_s} with an accuracy that matches the precision of theoretical calculations are thus necessary to check and further constrain theoretical methods.

Hadronic decays, $D_s^+ \to K^-K^+\pi^+$ and $D_s^+ \to \overline{K}^0K^+$, are the reference modes for the measurements of branching fractions of the D_s^+ decays to any other final state [2]. In addition, precise measurements of the absolute hadronic D_s^+ meson branching fractions improve our knowledge of the $B_{(s)}$ decays involving D_s^+, such as $B_{(s)}^0 \to D_s^{(*)-}D_{(s)}^{(*)+}$ [2], and of most of the other branching fraction measurements of B_s mesons performed at LHCb, like $B_s^0 \to \mu^+\mu^-$ [5]. For B_s-decay branching fraction measurements performed at LHCb,

[1] Charge conjugation is assumed throughout this paper unless stated otherwise.

JHEP09(2013)139

the key systematic uncertainty [24] is the ratio of fragmentation fractions f_s/f_d, whose experimental systematic error is dominated by $\mathcal{B}(D_s^+ \to K^-K^+\pi^+)$ [25, 26].[2] Normalization branching fractions, $\mathcal{B}(D_s^+ \to K^-K^+\pi^+)$ and $\mathcal{B}(D_s^+ \to \overline{K}^0K^+)$, have been measured so far only by CLEO [27] (see also the very recent update in ref. [28]). It is therefore important to provide new and independent measurements.

In this paper, we present results of absolute branching fraction measurements of $D_s^+ \to \mu^+\nu_\mu$ and $D_s^+ \to \tau^+\nu_\tau$ decays and perform a search for $D_s^+ \to e^+\nu_e$ decays. The measurement of $\mathcal{B}(D_s^+ \to \mu^+\nu_\mu)$ presented here supersedes the previous Belle measurement [14]. The analysis described here has a number of significant improvements, including an increased data sample and significantly improved inclusive D_s^+ reconstruction efficiency. The combined effect of these improvements and the accompanying change in the extraction of relevant signal yields results in a reduction of the expected error of $\mathcal{B}(D_s^+ \to \mu^+\nu_\mu)$ by more than a factor of two. The new analysis has improved systematic uncertainties. In addition, we present first measurements of absolute branching fractions of the D_s^+ normalization decays, $D_s^+ \to K^-K^+\pi^+$ and $D_s^+ \to \overline{K}^0K^+$, and of $D_s^+ \to \eta\pi^+$ decays. This analysis is based on a data sample of 913 fb^{-1} recorded at and near the $\Upsilon(4S)$ and $\Upsilon(5S)$ resonances — well above the open charm threshold — by the Belle detector at the KEKB asymmetric-energy collider [29, 30].

The rest of the paper is structured as follows. We describe the Belle detector and the data sample in section 2. In section 3, we present the method of measuring the absolute branching fraction of D_s^+ decays. The inclusive and exclusive event reconstruction steps are described in sections 4 and 5, respectively. Determination of the absolute branching fractions is discussed in section 6. Systematic uncertainties are itemized in section 7. We summarize our results in section 8 and conclude in section 9.

2 Belle detector and data sample

The data used in this analysis were collected with the Belle detector at the KEKB asymmetric energy e^+e collider. The Belle detector is a large-solid-angle magnetic spectrometer that consists of a silicon vertex detector (SVD), a 50-layer central drift chamber (CDC), an array of aerogel threshold Cherenkov counters (ACC), a barrel-like arrangement of time-of-flight scintillation counters (TOF), and an electromagnetic calorimeter (ECL) comprised of CsI(Tl) crystals located inside a superconducting solenoid coil that provides a 1.5 T magnetic field. An iron flux-return located outside of the coil is instrumented to detect K_L^0 mesons and to identify muons (KLM). The detector is described in detail elsewhere [1, 31]. Two inner detector configurations were used. A 2.0 cm diameter beampipe and a 3-layer silicon vertex detector was used for the first sample of 156 fb^{-1}, while a 1.5 cm diameter beampipe, a 4-layer silicon detector and a small-cell inner drift chamber were used to record the remaining 757 fb^{-1}.

Charged particles are reconstructed with the CDC and the SVD. Each is required to have an impact parameter with respect to the interaction point (IP) of less than 1.5 cm

[2] The fragmentation fractions, f_q, describe the probability that a b quark fragments in a B_q meson, where $q = d$ or s.

JHEP09(2013)139

along the beam direction (z) and less than 0.5 cm in the transverse ($r-\phi$) plane. A likelihood ratio for a given track to be a kaon or pion, $\mathcal{L}_{(K,\pi)}$, is obtained by utilizing specific ionization energy loss measurements in the CDC, light yield measurements from the ACC, and time-of-flight information from the TOF. For electron identification, we use position, cluster energy, and shower shape in the ECL, combined with track momentum and dE/dx measurements in the CDC and hits in the ACC. For muon identification, we extrapolate the CDC track to the KLM and compare the measured range and transverse deviation in the KLM with the expected values. Photons are detected with the ECL and are required to have energies in the laboratory frame of at least 50 (100) MeV in the ECL barrel (endcaps). Neutral pion candidates are reconstructed using photon pairs with an invariant mass between 120 and 150 MeV/c^2, which corresponds to $\pm 3.2\ \sigma$ around the nominal π^0 mass [2], where σ represents the invariant mass resolution. Neutral kaon candidates are reconstructed using charged pion pairs with an invariant mass within ± 20 MeV/c^2 ($\pm 5\ \sigma$) of the nominal K^0 mass.

We use Monte Carlo (MC) events generated with EVTGEN [32] and JETSET [33] and then processed through the detailed detector simulation implemented in GEANT3 [34]. QED final state radiation from charged particles is added during generation using the PHOTOS package [35]. The simulated samples for e^+e^- annihilation to $q\bar{q}$ ($q = u$, d, s, c, and b) are equivalent to six times the integrated luminosity of the data and are used to develop methods to separate signal events from backgrounds, identify types of background events, determine reconstruction efficiencies and the distributions needed for the extraction of the signal decays.

3 Method overview

The method of absolute branching fraction measurement of D_s^- decays is similar to the one previously used by Belle [14, 36] and BaBar [15]. In this method, the $e^+e^- \to c\bar{c}$ events that contain D_s^- mesons produced through the reactions

$$e^+e^- \to c\bar{c} \to D_{\rm tag} K_{\rm frag} X_{\rm frag} D_s^{*-}, \qquad D_s^{*-} \to D_s^- \gamma, \tag{3.1}$$

are fully reconstructed in two steps. In these events, one of the two charm quarks hadronizes into a D_s^{*-} meson while the other hadronizes into a tagging charm hadron, denoted $D_{\rm tag}$, that is one of D^0, D^+, Λ_c^+, D^{*+} or D^{*0}. The strangeness of the event is conserved by requiring an additional kaon, denoted $K_{\rm frag}$, be produced in the fragmentation process; $K_{\rm frag}$ is either K^+ or K_S^0. In events where Λ_c^+ is the tagging charm hadron, the baryon number of the event is conserved by requiring an anti-proton. Since Belle collected data at energies well above the $D_{\rm tag}^{(*)} K_{\rm frag} D_s^{*-}$ threshold, additional particles can be produced in the course of hadronization. These particles are denoted as $X_{\rm frag}$ and consist of an even number of kaons plus any number of pions or photons. In this measurement, only pions are considered when reconstructing the fragmentation system $X_{\rm frag}$.[3] We require

[3]The strangeness-conserving kaon and the baryon-number-conserving anti-proton are counted separately and are not included in the $X_{\rm frag}$ system.

JHEP09(2013)139

D_s^- mesons to be produced in a $D_s^{*-} \to D_s^- \gamma$ decay, which provides a powerful kinematic constraint that improves the resolution of the missing mass (defined below) and suppresses the combinatorial background.

In the first step of the measurement, no requirements are placed on the daughters of the signal D_s^- meson in order to obtain an inclusive sample of D_s^- events that is used for normalization in the calculation of the branching fractions. The number of inclusively reconstructed D_s^- mesons is extracted from the distribution of events in the missing mass, $M_{\rm miss}(D_{\rm tag}K_{\rm frag}X_{\rm frag}\gamma)$, recoiling against the $D_{\rm tag}K_{\rm frag}X_{\rm frag}\gamma$ system

$$M_{\rm miss}(D_{\rm tag}K_{\rm frag}X_{\rm frag}\gamma) = \sqrt{p_{\rm miss}(D_{\rm tag}K_{\rm frag}X_{\rm frag}\gamma)^2}, \tag{3.2}$$

where $p_{\rm miss}$ is the missing four-momentum in the event

$$p_{\rm miss}(D_{\rm tag}K_{\rm frag}X_{\rm frag}\gamma) = p_{e^+} + p_{e^-} - p_{D_{\rm tag}} - p_{K_{\rm frag}} - p_{X_{\rm frag}} - p_\gamma. \tag{3.3}$$

Here, p_{e^+} and p_{e^-} are the known four-momenta of the colliding positron and electron beams, respectively, and $p_{D_{\rm tag}}$, $p_{K_{\rm frag}}$, $p_{X_{\rm frag}}$, and p_γ are the measured four-momenta of the reconstructed $D_{\rm tag}$, strangeness-conserving kaon, fragmentation system and the photon from $D_s^{*-} \to D_s^-\gamma$, respectively. Correctly reconstructed events described in eq. (3.1) produce a peak in the $M_{\rm miss}(D_{\rm tag}K_{\rm frag}X_{\rm frag}\gamma)$ at the nominal D_s^- meson mass.

In the second step of the analysis, we search for the decay products of a specific D_s^- meson decay within the inclusive D_s^- meson sample reconstructed in the first step. In particular, we reconstruct purely leptonic $D_s^- \to e^-\overline{\nu}_e$, $D_s^- \to \mu^-\overline{\nu}_\mu$, and $D_s^- \to \tau^-\overline{\nu}_\tau$ decays within the inclusive D_s^- sample by requiring an additional charged track identified as an electron, muon or charged pion in the rest of the event. In the case of $D_s^- \to \tau^-\overline{\nu}_\tau$ decays, the electron, muon or pion identifies the subsequent tau decay to $e^-\overline{\nu}_e\nu_\tau$, $\mu^-\overline{\nu}_\mu\nu_\tau$ or $\pi^-\nu_\tau$, respectively. Hadronic decays, $D_s^- \to K^0K^-$ and $\eta\pi^-$, are reconstructed partially by explicitly requiring only the charged kaon or pion (originating directly from D_s^- meson decay) in the rest of the event but with no requirements on the neutral hadrons (K^0 or η) in order to increase the reconstruction efficiency. In the case of $D_s^- \to K^-K^+\pi^-$, all three charged tracks are required in the rest of the event. More details are given in section 5.

4 Inclusive $D_s^\pm$ reconstruction

The reconstruction of the inclusive $D_s^\pm$ sample starts with the reconstruction of the tagging charmed hadron, $D_{\rm tag}$. To maximize the reconstruction efficiency with reasonable purity, the ground-state $D_{\rm tag}$ hadrons (D^0, D^+, Λ_c^+) are reconstructed in the 18 hadronic decay modes listed in table 1. Only modes with up to one π^0 in the final state are used to avoid large backgrounds. If $D_{\rm tag}$ is reconstructed as Λ_c^+ baryon, an additional anti-proton is required in order to conserve the baryon number in the event.

The magnitude of the center-of-mass (CMS) momentum of the $D_{\rm tag}$ candidates is required to be greater than 2.3 GeV/c (or 2.5 GeV/c for the less clean $D_{\rm tag}$ modes) to reduce the combinatorial background and $e^+e^- \to B\overline{B}$ events. The decay products of the $D_{\rm tag}$ candidate are fitted to a common vertex; candidates with a poor fit quality are discarded by

JHEP09(2013)139

D^0 modes	$\mathcal{B}$ [%]
$K^-\pi^+$	3.9
$K^-\pi^+\pi^0$	13.9
$K^-\pi^+\pi^+\pi^-$	8.1
$K^-\pi^+\pi^+\pi^-\pi^0$	4.2
$K^0_S\pi^+\pi^-$	2.9
$K^0_S\pi^+\pi^-\pi^0$	5.4
Sum	38.4

D^+ modes	$\mathcal{B}$ [%]
$K^-\pi^+\pi^+$	9.4
$K^-\pi^+\pi^+\pi^0$	6.1
$K^0_S\pi^+$	1.5
$K^0_S\pi^+\pi^0$	6.9
$K^0_S\pi^+\pi^+\pi^-$	3.1
$K^+K^-\pi^+$	1.0
Sum	28.0

Λ_c^+ modes	$\mathcal{B}$ [%]
$pK^-\pi^+$	5.0
$pK^-\pi^+\pi^0$	3.4
pK^0_S	1.1
$\Lambda\pi^+$	1.1
$\Lambda\pi^+\pi^0$	3.6
$\Lambda\pi^+\pi^+\pi^-$	2.6
Sum	16.8

Table 1. Summary of $D_{\rm tag} = D^0$, D^+ and Λ_c^+ decay modes used in this measurement. The branching fractions are taken from ref. [2].

requiring χ^2/n.d.f. < 20, where n.d.f. is the number of degrees of freedom of the kinematic fit. The purity of the $D_{\rm tag}$ sample, given as a fraction of correctly reconstructed $D_{\rm tag}$ candidates, is rather low at this stage — around 17% in the signal region, defined as $\pm 3\ \sigma$ interval around the nominal $D_{\rm tag}$ mass, where σ is the $D_{\rm tag}$ decay-mode-dependent invariant mass resolution that ranges from 4 to 12 MeV/c^2. To further purify the $D_{\rm tag}$ sample, we train a NeuroBayes [37] neural network using a small sample of data (0.7% of the total sample). The network combines information from the following input variables into a single variable: the distance between the decay and the production vertices of the $D_{\rm tag}$ candidate in the $r-\phi$ plane, where the $D_{\rm tag}$ production vertex is defined by the intersection of its trajectory with the IP region; the χ^2/n.d.f. of the vertex fit of the $D_{\rm tag}$ candidate; the cosine of the angle between the $D_{\rm tag}$ momentum and the vector joining its decay and production vertices in the $r-\phi$ plane; for two-body decays, the cosine of the angle between the momentum of either $D_{\rm tag}$ daughter and the boost direction of the laboratory frame in the $D_{\rm tag}$ rest frame; the particle identification likelihood ratios; and, for the $D_{\rm tag}$ decay modes with a π^0, the smaller of the two photon energies. To obtain the signal and background distributions of the network's input variables, a statistical tool to unfold the data distributions ($_s\mathcal{P}$lot [38]) is applied. Network is then applied to the complementary subsample (again representing around 0.7% of the total sample) that we use to optimize the selection on the network output variable for each $D_{\rm tag}$ mode individually by maximizing $S/\sqrt{S+B}$, where S (B) refers to the signal (background) yield in the signal window of $D_{\rm tag}$ invariant mass determined by performing a fit to the $D_{\rm tag}$ invariant mass distribution.[4] After the optimization, the purity of the correctly reconstructed $D_{\rm tag}$ candidates increases from 17% to 42% while only 16% of signal $D_{\rm tag}$ candidates is lost. We retain only $D_{\rm tag}$ candidates from the signal region of the $D_{\rm tag}$ invariant mass in the rest of the analysis.

Once the ground-state $D_{\rm tag}$ hadrons have been reconstructed, D^0 and D^+ mesons originating from D^* decays are identified by reconstructing the decays $D^{*+} \to D^0\pi^+$, $D^+\pi^0$, and $D^{*0} \to D^0\pi^0$, $D^0\gamma$. We do this to purify the subsequent $K_{\rm frag}X_{\rm frag}\gamma$ reconstruction:

[4]This approach avoids a bias of the selection originating from statistical fluctuations possibly learned by the network. Since the optimization of $D_{\rm tag}$'s selection is performed using a very small fraction of data, any bias that could be triggered by statistical fluctuations is negligible.

JHEP09(2013)139

by absorbing one more particle into the tagging charm hadron, the subsequent combinatorial background is reduced. In addition, by reconstructing $D^{*+} \to D^0\pi^+$ decays, we can determine the flavor or charm quantum number of D^0 or $\overline{D}^0$ candidates reconstructed in final states with a K^0_S. The pion from the D^* decay is refitted to the D production vertex to improve the resolution of the mass difference, $\Delta M = M(D\pi) - M(D)$. The laboratory frame energy of the photon(s) originating from the π^0 produced in $D^* \to D\pi^0$ (produced directly in $D^{*0} \to D^0\gamma$) is required to be larger than 50 (175) MeV. In the $D^0\gamma$ final state, the γ candidate is combined with each other photon and, if the two-photon invariant mass is within 10 MeV/c^2 around the nominal π^0 mass and their energy asymmetry $((E_{\gamma_1} - E_{\gamma_2})/(E_{\gamma_1} + E_{\gamma_2}))$ is smaller than 0.5, the D^{*0} candidate is rejected. For all D^* decays, the mass difference, ΔM, is required to be within 3 σ of the corresponding nominal mass difference.

For strangeness conserving kaon candidate, $K_{\rm frag}$, all $K^\pm$ or K^0_S candidates that do not overlap with the $D_{\rm tag}$ candidate are considered.

From the remaining tracks and π^0 candidates in the event that do not overlap with the $D_{\rm tag}K_{\rm frag}$ candidate, we form the $X_{\rm frag}$ candidates. Only modes with up to three pions and up to one π^0 are used to suppress the combinatorial background. In addition, pions must have a momentum above 100 MeV/c in the laboratory frame. At this stage, no requirement is applied to the total charge of the $X_{\rm frag}$ system.

The $D_{\rm tag}$, $X_{\rm frag}$ and $K_{\rm frag}$ candidates are combined to form $D_{\rm tag}K_{\rm frag}X_{\rm frag}$ combinations. We keep only combinations with total charge ±1; these constitute the inclusive sample of $D_s^{*\mp}$ mesons. The charm and strange quark content of the $D_{\rm tag}K_{\rm frag}X_{\rm frag}$ system is required to be consistent with that recoiling from a D_s^*: if $D_{\rm tag}$ is reconstructed in a flavor-specific decay mode and $K_{\rm frag}$ is charged, the kaon charge and the charm quantum number of $D_{\rm tag}$ must be opposite the D_s^* charge; if $K_{\rm frag}$ is neutral the charm quantum number of $D_{\rm tag}$ must be opposite the D_s^* charge; and if $D_{\rm tag}$ is reconstructed in a self-conjugate decay mode, the charge of $K_{\rm frag}$ must be opposite the D_s^* charge. All other candidates are rejected. A kinematic fit to $D_{\rm tag}K_{\rm frag}X_{\rm frag}$ candidates is performed in which the particles are required to originate from a common point within the IP region and the $D_{\rm tag}$ mass is constrained to its nominal value. We select only one $D_{\rm tag}K_{\rm frag}X_{\rm frag}$ candidate per event that has its missing mass, $M_{\rm miss}(D_{\rm tag}K_{\rm frag}X_{\rm frag}) = \sqrt{|p_{e^+} + p_{e^-} - p_{D_{\rm tag}} - p_{K_{\rm frag}} - p_{X_{\rm frag}}|^2}$, closest to the nominal D_s^{*+} mass and between 2.00 and 2.25 GeV/c^2, which corresponds to a ±3 σ interval.

Finally, a photon candidate is identified that is consistent with the decay $D_s^{*\pm} \to D_s^\pm\gamma$ and does not overlap with the $D_{\rm tag}K_{\rm frag}X_{\rm frag}$ system. We require that the energy of the photon candidate be larger than 120 MeV in the laboratory frame and that the cosine of the angle between the CMS momenta of the $D_{\rm tag}$ hadron and the photon candidate be negative, since the signal photon should be in the hemisphere opposite the $D_{\rm tag}$ hadron. We perform a similar kinematic fit with the signal photon included and with the missing mass recoiling against the $D_{\rm tag}K_{\rm frag}X_{\rm frag}$ system constrained to the nominal D_s^{*+} mass. All $D_{\rm tag}K_{\rm frag}X_{\rm frag}\gamma$ candidates are required to have a CMS momentum larger than 2.8 GeV/c and $M_{\rm miss}(D_{\rm tag}K_{\rm frag}X_{\rm frag}\gamma) > 1.83$ GeV/c^2 (see eq. (3.2)). After the final selections, there

JHEP09(2013)139

are an average of 2.1 $D_{\rm tag}K_{\rm frag}X_{\rm frag}\gamma$ candidates per event; these are due solely to multiple γ candidates. Among these, we select the one with the highest NeuroBayes network output that is trained to separate signal photons from others based on photon energy, the detecting region of the ECL (forward, barrel or backward region), the ratio of the energies summed in 3×3 and 5×5 ECL crystals in the transverse plane around the crystal with the largest energy deposit, the invariant mass of the combination of the photon candidate with any other photon candidate that is closest to the π^0 nominal mass, the energy asymmetry of this two-photon combination, and the invariant mass and energy asymmetry of the two-photon combination whose invariant mass is second closest to the nominal π^0 mass. A relative gain of 23% in absolute reconstruction efficiency is obtained by applying the best $D_{\rm tag}K_{\rm frag}X_{\rm frag}\gamma$ candidate selection instead of a completely random selection. Figure 1 shows the distributions of $M_{\rm miss}(D_{\rm tag}K_{\rm frag}X_{\rm frag}\gamma)$ for each $X_{\rm frag}$ mode.

4.1 Inclusive D_s^+ yield extraction

The yield of inclusively reconstructed D_s^+ mesons is determined by performing a χ^2 fit to the missing mass $M_{\rm miss}(D_{\rm tag}K_{\rm frag}X_{\rm frag}\gamma)$ distribution for each $X_{\rm frag}$ mode. The events fall into six categories: signal candidates; mis-reconstructed signal candidates, where either $K_{\rm frag}$ or one of the pions forming the $X_{\rm frag}$ system originates in reality from a D_s^+ decay; background candidates where the signal γ candidate originates from $D^{*0}\to D^0\gamma$ decays; background candidates where the signal γ originates from the π^0 produced in $D^*_{(s)}\to D_{(s)}\pi^0$ decays; background candidates with a bad γ — the energy deposited in the ECL being produced by an unmatched charged track or by a beam-induced interaction; and background candidates where the signal γ originates from a π^0 that does not itself originate from a $D^*_{(s)}$ decay. Each of the six categories is represented with a smoothed non-parametric histogram [39] probability density function (PDF), $\mathcal{H}(M_{\rm miss}(D_{\rm tag}K_{\rm frag}X_{\rm frag}\gamma))$, taken from a large sample of MC events. The fit function for a given $X_{\rm frag}$ mode is written as

$$\begin{aligned}\mathcal{F}^{X_{\rm frag}}(M_{\rm miss}(D_{\rm tag}K_{\rm frag}X_{\rm frag}\gamma)) = N_{\rm sig}^{X_{\rm frag}}\mathcal{H}_{\rm sig}^{X_{\rm frag}}(M_{\rm miss}(D_{\rm tag}K_{\rm frag}X_{\rm frag}\gamma)-\delta_{M_{\rm miss}})\otimes\mathcal{G}(\sigma_{\rm cal})\\ +\sum_{i=1}^{5}N_i^{X_{\rm frag}}\mathcal{H}_i^{X_{\rm frag}}(M_{\rm miss}(D_{\rm tag}K_{\rm frag}X_{\rm frag}\gamma)),\end{aligned}\tag{4.1}$$

where N represents the yield of each component and the first (second) term describes the contribution of signal (the sum of the five background components). The histogram PDF of the signal, $\mathcal{H}_{\rm sig}^{X_{\rm frag}}(M_{\rm miss}(D_{\rm tag}K_{\rm frag}X_{\rm frag}\gamma)-\delta_{M_{\rm miss}})$, is numerically convolved with a Gaussian function, $\mathcal{G}(\sigma_{\rm cal})$, centered at zero and with width $\sigma_{\rm cal}$, which takes into account possible differences between $M_{\rm miss}(D_{\rm tag}K_{\rm frag}X_{\rm frag}\gamma)$ resolutions in the data and MC samples. The calibration of $\sigma_{\rm cal}$ is described in the next paragraph. The position of the signal peak in data relative to the position in the MC, $\delta_{M_{\rm miss}}$, is a free parameter of the fit. We also float all normalization parameters, $N_i^{X_{\rm frag}}$, except the normalization of the background component where the signal γ candidate originates from $D^{*0}\to D^0\gamma$ decays, which is fixed relative to the more abundant and similar background component where the signal γ candidate originates from the π^0 produced in $D^{*0}_{(s)}\to D_{(s)}\pi^0$ decays. The fraction $f_{D^0\gamma/D_{(s)}\pi^0}$ is fixed to the value obtained in the MC sample.

JHEP09(2013)139

$X_{\rm frag}$ mode	$N_{D_s}^{\rm inc}$
nothing	23460 ± 280
$\pi^{\pm}$	23390 ± 350
π^0	8030 ± 480
$\pi^{\pm}\pi^0$	9290 ± 550
$\pi^{\pm}\pi^{\mp}$	14930 ± 450
$\pi^{\pm}\pi^{\mp}\pi^{\pm}$	5680 ± 330
$\pi^{\pm}\pi^{\mp}\pi^0$	9580 ± 820
Sum	94360 ± 1310

Table 2. Yields of inclusively reconstructed $D_s^{\pm}$ mesons per individual $X_{\rm frag}$ mode. The uncertainties are statistical only.

We calibrate the $M_{\rm miss}(D_{\rm tag}K_{\rm frag}X_{\rm frag}\gamma)$ resolution using the mass difference between D_s^{*+} and D_s^+, $\Delta M = M_{D_s^{*+}} - M_{D_s^+}$, for exclusively reconstructed $D_s^{*+} \to D_s^+\gamma$ decays, where D_s^+ decays to $\phi\pi^+$ and $\phi \to K^+K^-$. In the exclusive reconstruction of D_s^{*+} mesons, the same requirements are used for the signal photon candidate as in the inclusive reconstruction. The dominant contribution to the ΔM and $M_{\rm miss}(D_{\rm tag}K_{\rm frag}X_{\rm frag}\gamma)$ resolutions is the signal photon energy resolution. In the former case, the smearing of the D_s^+ momentum cancels almost completely in the mass difference while, in the latter case, the impact of experimental smearing of $p_{\rm miss}(D_{\rm tag}K_{\rm frag}X_{\rm frag})$ on $M_{\rm miss}(D_{\rm tag}K_{\rm frag}X_{\rm frag}\gamma)$ is minimized by performing a mass constrained vertex fit of $D_{\rm tag}K_{\rm frag}X_{\rm frag}$ candidates to the nominal D_s^{*+} mass. According to the MC study, the ΔM and $M_{\rm miss}(D_{\rm tag}K_{\rm frag}X_{\rm frag}\gamma)$ resolutions are the same to within a few percent, which justifies the calibration of the $M_{\rm miss}(D_{\rm tag}K_{\rm frag}X_{\rm frag}\gamma)$ resolution by comparing ΔM resolutions of exclusively reconstructed $D_s^{*+} \to D_s^+\gamma$ decays obtained from data and MC. We parameterize the contribution of correctly reconstructed $D_s^{*+} \to D_s^+\gamma$ decays in ΔM as in the case of the signal parameterization of $M_{\rm miss}(D_{\rm tag}K_{\rm frag}X_{\rm frag}\gamma)$ as a histogram PDF convolved with a Gaussian function, $\mathcal{H}_{\rm sig}(\Delta M - \delta_{\Delta M}) \otimes \mathcal{G}(\sigma_{\rm cal})$, where $\delta_{\Delta M}$ is the difference between the peak positions in data and MC. The background shape is fitted by a second order polynomial. We achieve best agreement between data and simulated ΔM distributions when $\sigma_{\rm cal} = 2.0 \pm 0.2$ MeV/c^2.

The fitted inclusive $D_s^{\pm}$ yields for each $X_{\rm frag}$ mode are given in table 2. The PDFs describe well the observed data distributions as can be seen from the normalized fit residuals in figure 1. The normalized χ^2 values of the fits are between 1.06 and 1.32.

In the fit to the $M_{\rm miss}(D_{\rm tag}K_{\rm frag}X_{\rm frag}\gamma)$ distributions, we set $\sigma_{\rm cal} = 2.0$ MeV/c^2. To estimate the systematic uncertainty, we repeat the fits to the $M_{\rm miss}(D_{\rm tag}K_{\rm frag}X_{\rm frag}\gamma)$ distributions by changing $\sigma_{\rm cal}$ by ± 0.2 MeV/c^2 (one standard deviation) and assign the resulting difference of $\pm 1.39\%$ in the inclusive $D_s^{\pm}$ yield as the systematic error. In the nominal fit, the fraction $f_{D^0\gamma/D_{(s)}\pi^0}$ is fixed to the MC-determined value. We vary this parameter by $\pm 5\%$ to conservatively estimate the possible differences between data and MC in the relative production rates of D^{*+} and D^{*0} mesons. The impact on the inclusive $D_s^{\pm}$ yields is found to be small ($\pm 0.41\%$). To account for the limited statistics of the MC sample

JHEP09(2013)139

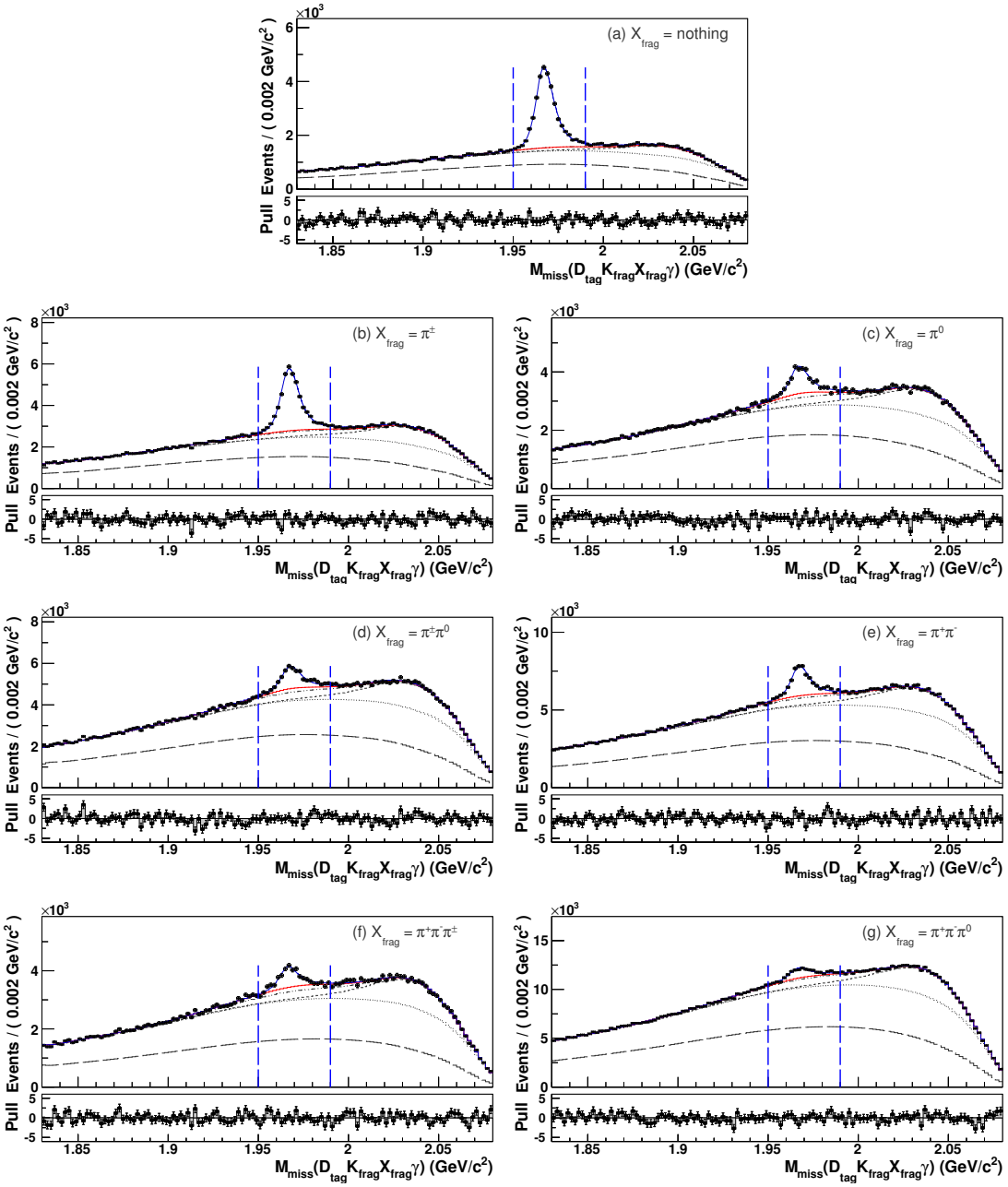

Figure 1. The $M_{\rm miss}(D_{\rm tag}K_{\rm frag}X_{\rm frag}\gamma)$ distributions for all seven $X_{\rm frag}$ modes with superimposed fit results (solid blue line). Within each panel, the curves show, from bottom to top, the cumulative contributions of background candidates where the signal γ originates from a π^0 that does not itself originate from a $D^*_{(s)}$ decay, background candidates with wrong γ, background candidates where the signal γ originates from a π^0 decay produced in $D^*_{(s)} \to D_{(s)}\pi^0$ decays, background candidates where the signal γ candidate originates from a $D^{*0} \to D^0\gamma$ decays or mis-reconstructed signal candidates, and signal candidates. The two blue dashed vertical lines indicate the $M_{\rm miss}(D_{\rm tag}K_{\rm frag}X_{\rm frag}\gamma)$ signal region. The normalized fit residual (referred in this and all other figures as "Pull") is defined as $(N_{\rm observed} - N_{\rm fit})/\sqrt{N_{\rm observed}}$.

JHEP09(2013)139

used to determine the histogram PDFs, we repeatedly vary the contents of all bins of all histogram templates within their statistical uncertainties and refit. The systematic uncertainty is taken to be the root mean square (RMS) of the obtained distribution of the inclusive signal yield ($\pm 0.51\%$).

The total inclusive $D_s^\pm$ yield, including systematic uncertainties, is

$$N_{D_s}^{\rm inc} = 94360 \pm 1310(\text{stat.}) \pm 1450(\text{syst.}). \tag{4.2}$$

5 Reconstruction of D_s^+ decays within the inclusive D_s^+ sample

Using the inclusive sample of D_s^+ mesons, we reconstruct specific D_s^+ meson decays to the following final states: $K^-K^+\pi^+$, $\overline{K}^0K^+$, $\eta\pi^+$, $e^+\nu_e$, $\mu^+\nu_\mu$, and $\tau^+\nu_\tau$; for the last mode, the τ lepton is reconstructed via its decays to $e^+\nu_e\overline{\nu}_\tau$, $\mu^+\nu_\mu\overline{\nu}_\tau$, and $\pi^+\overline{\nu}_\tau$. We keep only inclusive D_s^+ candidates within the signal region of $M_{\rm miss}(D_{\rm tag}K_{\rm frag}X_{\rm frag}\gamma)$ defined as $1.95\ \text{GeV}/c^2 < M_{\rm miss}(D_{\rm tag}K_{\rm frag}X_{\rm frag}\gamma) < 1.99\ \text{GeV}/c^2$; the sideband regions are used to study background properties except in the case of the $D_s^+ \to K^-K^+\pi^+$ decay, where all inclusive D_s^+ candidates are kept. We find that 88.7% of correctly reconstructed inclusive D_s^+ candidates populate the $M_{\rm miss}(D_{\rm tag}K_{\rm frag}X_{\rm frag}\gamma)$ signal region, within which the purity of the inclusive D_s^+ sample ranges between 3.5% ($X_{\rm frag} = \pi^\pm\pi^\mp\pi^0$) and 41% ($X_{\rm frag} = $ nothing).

In the following subsections, we describe the reconstruction procedure and signal yield extraction for the six decay modes.

5.1 $D_s^+ \to K^-K^+\pi^+$

The reconstruction of $D_s^+ \to K^-K^+\pi^+$ decays requires exactly three charged tracks in the rest of the event with a net charge equal to the charge of the inclusively reconstructed D_s^+ candidate. The track with charge opposite that of the inclusive D_s^+ candidate is selected to be the K^- candidate while the two same-sign tracks are identified as K^+ or π^+ based on their likelihood ratios, $\mathcal{L}_{K,\pi}$.

The exclusively reconstructed $D_s^+ \to K^-K^+\pi^+$ candidates within the inclusive D_s^+ sample are identified as a peak at the nominal mass of the D_s^{*+} in the invariant mass distribution of the $K^-K^+\pi^+\gamma$ combination, $M(K^-K^+\pi^+\gamma)$. Here, γ stands for the signal photon candidate used to reconstruct the inclusive D_s^+ candidate in the recoil against the $D_{\rm tag}K_{\rm frag}X_{\rm frag}\gamma$ system. The $M(K^-K^+\pi^+\gamma)$ is chosen over the D_s^+ invariant mass, $M(K^-K^+\pi^+)$, because both sides — inclusive and exclusive — have to be correctly reconstructed to produce peaks in $M(K^-K^+\pi^+\gamma)$ and $M_{\rm miss}(D_{\rm tag}K_{\rm frag}X_{\rm frag}\gamma)$. Correctly reconstructed $D_s^+ \to K^-K^+\pi^+$ events will peak in $M(K^-K^+\pi^+)$ even if the inclusive reconstruction of D_s^+ candidates fails, e.g., the photon candidate is incorrectly identified. The $M(K^-K^+\pi^+\gamma)$ and $M_{\rm miss}(D_{\rm tag}K_{\rm frag}X_{\rm frag}\gamma)$ are correlated due to their common input: the photon four-momentum. Imposing the requirement that inclusive D_s^+ candidates populate the signal $M_{\rm miss}(D_{\rm tag}K_{\rm frag}X_{\rm frag}\gamma)$ region would distort the background distribution to have a peaking structure in $M(K^-K^+\pi^+\gamma)$. We avoid this by taking all inclusive D_s^+ candidates into consideration rather than only those populating the signal region in $M_{\rm miss}(D_{\rm tag}K_{\rm frag}X_{\rm frag}\gamma)$.

JHEP09(2013)139

We parameterize the $M(K^-K^+\pi^+\gamma)$ distribution as

$$\begin{aligned}\mathcal{F}(M(K^-K^+\pi^+\gamma)) = & N_{\rm sig}\cdot\mathcal{H}_{\rm sig}(M(K^-K^+\pi^+\gamma)-\delta_M)\otimes\mathcal{G}(\sigma_{\rm cal}^{\rm excl}) \\ & + N_{D_s^*\pi^0}\cdot\mathcal{H}_{D_s^*\pi^0}(M(K^-K^+\pi^+\gamma)) \\ & + N_{\rm comb}\cdot\big[1+c_1\cdot M(K^-K^+\pi^+\gamma) \\ & + c_2\cdot M(K^-K^+\pi^+\gamma)^2+c_3\cdot M(K^-K^+\pi^+\gamma)^3\big]\,, \end{aligned} \tag{5.1}$$

where the three terms describe correctly reconstructed $D_s^{*+}\to D_s^+\gamma\to K^-K^+\pi^+\gamma$ decays (signal), mis-reconstructed $D_s^{*+}\to D_s^+\pi^0\to K^-K^+\pi^+\gamma\gamma$ decays where one of the photons from the π^0 decay is lost, and random combinations of charged tracks or photon (combinatorial background). The latter is parameterized as a third order polynomial while the first two contributions are represented using the non-parametric histogram PDFs taken from MC. We convolve the signal histogram PDF with a Gaussian function, $\mathcal{G}(\sigma_{\rm cal}^{\rm excl})$, to take into account the differences between the resolutions of $M(K^-K^+\pi^+\gamma)$ in real and MC samples. We estimate $\sigma_{\rm cal}^{\rm excl}$ by the procedure described in section 4.1, the only difference being that the resolution on $M(K^-K^+\pi^+\gamma)$ is calibrated instead of the D_s^{*+} and D_s^+ mass difference. We determine $\sigma_{\rm cal}^{\rm excl}=3.2\pm0.2$ MeV/c^2. Free parameters of the fit are the normalization parameters, N_i, the position of the signal peak relative to the peak position in the MC, δ_M, and the combinatorial background shape parameters, c_i.

The $M(K^-K^+\pi^+\gamma)$ distribution of exclusively reconstructed $D_s^+\to K^-K^+\pi^+$ decays within the inclusive D_s^+ sample is shown in figure 2 with the superimposed fit. The number of correctly reconstructed $D_s^+\to K^-K^+\pi^+$ decays is

$$N(D_s^+\to K^-K^+\pi^+)=4094\pm123, \tag{5.2}$$

where the error is statistical only.

5.2 $D_s^+\to\overline{K}^0K^+$

We reconstruct $D_s^+\to\overline{K}^0K^+$ decays by requiring only one additional charged kaon in the rest of the event whose charge equals that of the inclusively reconstructed D_s^+ candidate. The neutral kaon is not reconstructed; rather, it is identified as a peak at the nominal mass-squared of the neutral kaon in the missing-mass-squared distribution

$$M^2_{\rm miss}(D_{\rm tag}K_{\rm frag}X_{\rm frag}\gamma K)=p^2_{\rm miss}(D_{\rm tag}K_{\rm frag}X_{\rm frag}\gamma K),$$

where the missing four-momentum is given by

$$p_{\rm miss}(D_{\rm tag}K_{\rm frag}X_{\rm frag}\gamma K)=p_{e^+}+p_{e^-}-p_{D_{\rm tag}}-p_{K_{\rm frag}}-p_{X_{\rm frag}}-p_\gamma-p_K.$$

An explicit reconstruction of the $\overline{K}^0$ meson to two oppositely charged pions would lead to a significant signal loss. The signal peak of $D_s^+\to\overline{K}^0K^+$ in the $M^2_{\rm miss}(D_{\rm tag}K_{\rm frag}X_{\rm frag}\gamma K)$ distribution is used to calibrate the $M^2_{\rm miss}$ resolution, which is important in the extraction of the signal yield of $D_s^+\to\mu^+\nu_\mu$ decays. Since the flavor of the neutral kaon is not determined, the doubly Cabibbo suppressed decays, $D_s^+\to K^0K^+$, also contribute to the peak in $M^2_{\rm miss}(D_{\rm tag}K_{\rm frag}X_{\rm frag}\gamma K)$. Their relative contribution can be estimated naively to

JHEP09(2013)139

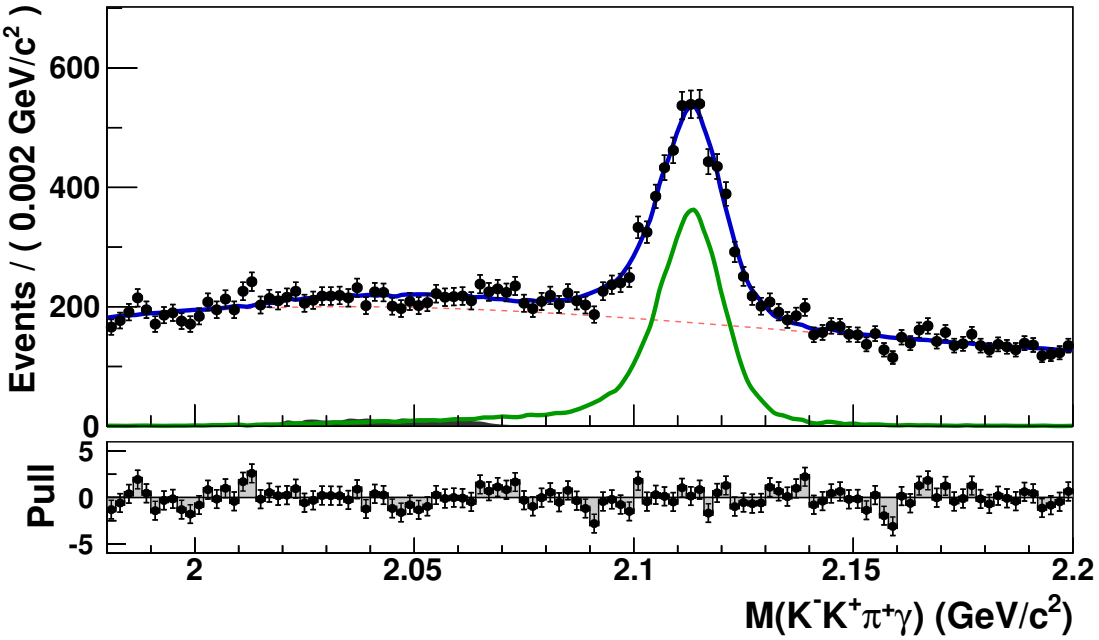

Figure 2. The $M(K^-K^+\pi^+\gamma)$ distribution of exclusively reconstructed $D_s^+ \to K^-K^+\pi^+$ decays within the inclusive D_s^+ sample with superimposed fit results (solid blue line). The solid green line shows the signal contribution while the red dashed line shows the contribution of combinatorial background; the contribution of $D_s^+ \to K^-K^+\pi^-$ candidates originating from $D_s^{*+} \to D_s^+\pi^0$ is indicated by the full dark gray histogram.

be equal to $\tan^4\theta_C \approx 0.29\%$ (θ_C being the Cabibbo mixing angle), which is an order of magnitude below the expected statistical uncertainty and thus safely neglected.

The signal yield of partially reconstructed $D_s^+ \to \overline{K}^0K^+$ decays is extracted by performing a binned extended maximum likelihood fit to the $M^2_{\rm miss}(D_{\rm tag}K_{\rm frag}X_{\rm frag}\gamma K)$ distribution. The signal component is parameterized as a sum of three Gaussian functions with a common mean. In the fit, we fix the signal shape parameters to the values determined from the MC sample except for the mean and the resolution scaling factor, s, of the core and the second Gaussian function. In addition to the signal contribution, two-body $D_s^+ \to \pi^0K^+$ and $D_s^+ \to \eta K^+$ decays peak in the $M^2_{\rm miss}(D_{\rm tag}K_{\rm frag}X_{\rm frag}\gamma K)$ distribution. We use the same parameterization for these peaking backgrounds as for signal except that we fix their means to the nominal masses squared of π^0 and η mesons. Other background sources that produce distinct structures in $M^2_{\rm miss}(D_{\rm tag}K_{\rm frag}X_{\rm frag}\gamma K)$ are: $D_s \to K^{*+}\overline{K}^0 \to K^+\pi^0\overline{K}^0$ decays and $D_s^+ \to \eta\pi^+$ decays where the π^+ is misidentified as signal K^+ candidate. Both contributions are parameterized as the sum of a Gaussian and a bifurcated Gaussian function, where all parameters are fixed to the values determined from the MC sample. The combinatorial background is parameterized with a fourth-order polynomial whose coefficients are determined with the fit to the $M^2_{\rm miss}(D_{\rm tag}K_{\rm frag}X_{\rm frag}\gamma K)$ distribution for inclusive D_s^+ candidates in the $M_{\rm miss}(D_{\rm tag}K_{\rm frag}X_{\rm frag}\gamma) < 1.95$ GeV/c^2 sideband region. Yields of all but two event categories are free parameters of the fit; the $D_s^+ \to \eta K^+$ and $D_s^+ \to \eta\pi^+$ yields are constrained to the expected values based on their known branching fractions and MC determined efficiencies.

JHEP09(2013)139

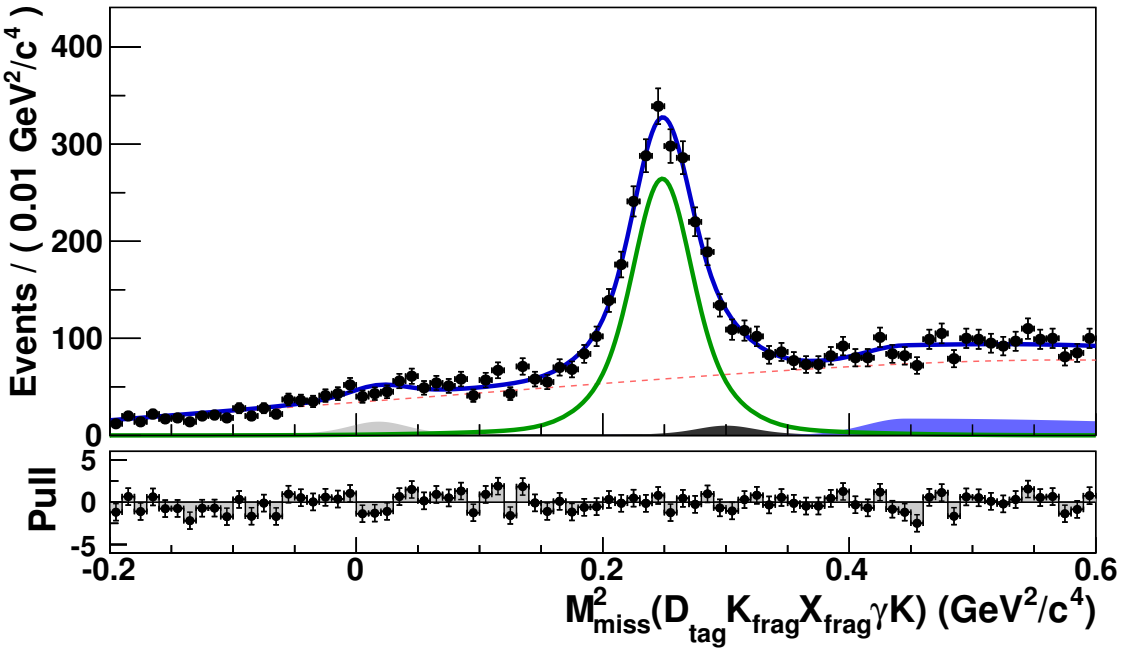

Figure 3. The $M^2_{\rm miss}(D_{\rm tag}K_{\rm frag}X_{\rm frag}\gamma K)$ distribution of partially reconstructed $D_s^+ \to \overline{K}^0K^+$ decays within the inclusive D_s^+ sample with superimposed fit results (solid blue line). The solid green line shows the signal contribution, the dashed red line the contribution of combinatorial background, while the full histograms show the contributions of $D_s^+ \to \pi^0K^+$ (light gray), $D_s^+ \to \eta K^+$ (dark gray) or $D_s^+ \to K^{*+}\overline{K}^0$ decays (blue).

The $M^2_{\rm miss}(D_{\rm tag}K_{\rm frag}X_{\rm frag}\gamma K)$ distribution of partially reconstructed $D_s^+ \to \overline{K}^0K^+$ decays within the inclusive D_s^+ sample is shown in figure 3 with the superimposed fit. The number of correctly reconstructed $D_s^+ \to \overline{K}^0K^+$ decays is

$$N(D_s^+ \to \overline{K}^0K^+) = 2018 \pm 75, \tag{5.3}$$

where the error is statistical only. The yield of Cabibbo suppressed $D_s^+ \to \pi^0K^+$ decays, 108 ± 31 (statistical error only), is found to be consistent within uncertainties with the expectation, 52 ± 18, based on a measurement performed by CLEO [40].

5.3 $D_s^+ \to \eta\pi^+$

As in the case of $D_s^+ \to \overline{K}^0K^+$ decays, we perform a partial reconstruction of $D_s^+ \to \eta\pi^+$ decays. We require only one charged track consistent with the pion hypothesis in the rest of the event. To avoid a significant signal loss, we do not perform an explicit reconstruction of the η meson but rather identify it as a peak at the nominal mass-squared of the η in the missing-mass-squared distribution

$$M^2_{\rm miss}(D_{\rm tag}K_{\rm frag}X_{\rm frag}\gamma\pi) = p^2_{\rm miss}(D_{\rm tag}K_{\rm frag}X_{\rm frag}\gamma\pi),$$

where the missing four-momentum is given by

$$p_{\rm miss}(D_{\rm tag}K_{\rm frag}X_{\rm frag}\gamma\pi) = p_{e^+} + p_{e^-} - p_{D_{\rm tag}} - p_{K_{\rm frag}} - p_{X_{\rm frag}} - p_\gamma - p_\pi.$$

JHEP09(2013)139

The sample of events with inclusive D_s^+ candidate plus one additional positively charged pion contains a significant contribution of $D_s^+ \to \tau^+\nu_\tau$ decays with the tau lepton decaying hadronically to a charged pion and a neutrino. The contribution of these events is suppressed by requiring that the extra neutral energy in the ECL ($E_{\rm ECL}$) be larger than 1.0 GeV, where $E_{\rm ECL}$ represents the sum over all energy deposits in the ECL that are not associated with the charged pion candidate and the tracks and neutrals used in the inclusive reconstruction of the D_s^+ candidate [3]. The $D_s^+ \to \tau^+\nu_\tau \to \pi^+\overline{\nu}_\tau\nu_\tau$ decays peak at zero in $E_{\rm ECL}$ while $D_s^+ \to \eta\pi^+$ decays deposit a significant amount of energy in the ECL via the η decay products. (See section 5.5 for more details.)

The signal yield of partially reconstructed $D_s^+ \to \eta\pi^+$ decays is extracted by performing a binned maximum likelihood fit to the $M^2_{\rm miss}(D_{\rm tag}K_{\rm frag}X_{\rm frag}\gamma\pi)$ distribution. We use the same parameterization for the signal component as in the case of $D_s^+ \to \overline{K}^0K^+$ decays. In addition, the resolution scaling factor of the core and the second Gaussian, s, is allowed to float within a Gaussian constraint in the fit, where the mean and width of the constraint are set to the value and uncertainty determined in the fit of the $D_s^+ \to \overline{K}^0K^+$ candidates ($s = 1.177 \pm 0.052$), respectively. We identify a single source of peaking background to be the two-body $D_s^+ \to K^0\pi^+$ decay that peaks at the neutral kaon mass-squared and is parameterized in the same way as the signal. Other background sources that produce distinct structures in $M^2_{\rm miss}(D_{\rm tag}K_{\rm frag}X_{\rm frag}\gamma\pi)$ are $D_s^+ \to \overline{K}^0K^+$ decays with a misidentified kaon and $D_s^+ \to \rho^0K^+ \to \pi^+\pi^-K^+$ decays; both are parameterized as bifurcated Gaussian functions. The combinatorial background is parameterized with a fourth order polynomial whose coefficients are fixed to the values determined with the fit to the $M^2_{\rm miss}(D_{\rm tag}K_{\rm frag}X_{\rm frag}\gamma\pi)$ distribution of inclusive D_s^+ candidates from the $M_{\rm miss}(D_{\rm tag}K_{\rm frag}X_{\rm frag}\gamma) < 1.95$ GeV/c^2 sideband region. Yields of all but two event categories are free parameters of the fit; the $D_s^+ \to K^0\pi^+$ and $D_s^+ \to \overline{K}^0K^+$ yields are constrained to expected values based on their known branching fractions and MC-determined efficiencies.

The $M^2_{\rm miss}(D_{\rm tag}K_{\rm frag}X_{\rm frag}\gamma\pi)$ distribution is shown in figure 4 with the superimposed fit. The number of correctly reconstructed $D_s^+ \to \eta\pi^+$decays is

$$N(D_s^+ \to \eta\pi^+) = 788 \pm 59, \tag{5.4}$$

where the error is statistical only.

5.4 $D_s^+ \to \mu^+\nu_\mu$

The $D_s^+ \to \mu^+\nu_\mu$ decays are reconstructed by requiring one additional charged track consistent with the muon hypothesis in the rest of the event. The single missing neutrino is then identified as a peak at zero in the missing-mass-squared distribution

$$M^2_{\rm miss}(D_{\rm tag}K_{\rm frag}X_{\rm frag}\gamma\mu) = p^2_{\rm miss}(D_{\rm tag}K_{\rm frag}X_{\rm frag}\gamma\mu),$$

where the missing four-momentum is given by

$$p_{\rm miss}(D_{\rm tag}K_{\rm frag}X_{\rm frag}\gamma\mu) = p_{e^+} + p_{e^-} - p_{D_{\rm tag}} - p_{K_{\rm frag}} - p_{X_{\rm frag}} - p_\gamma - p_\mu.$$

JHEP09(2013)139

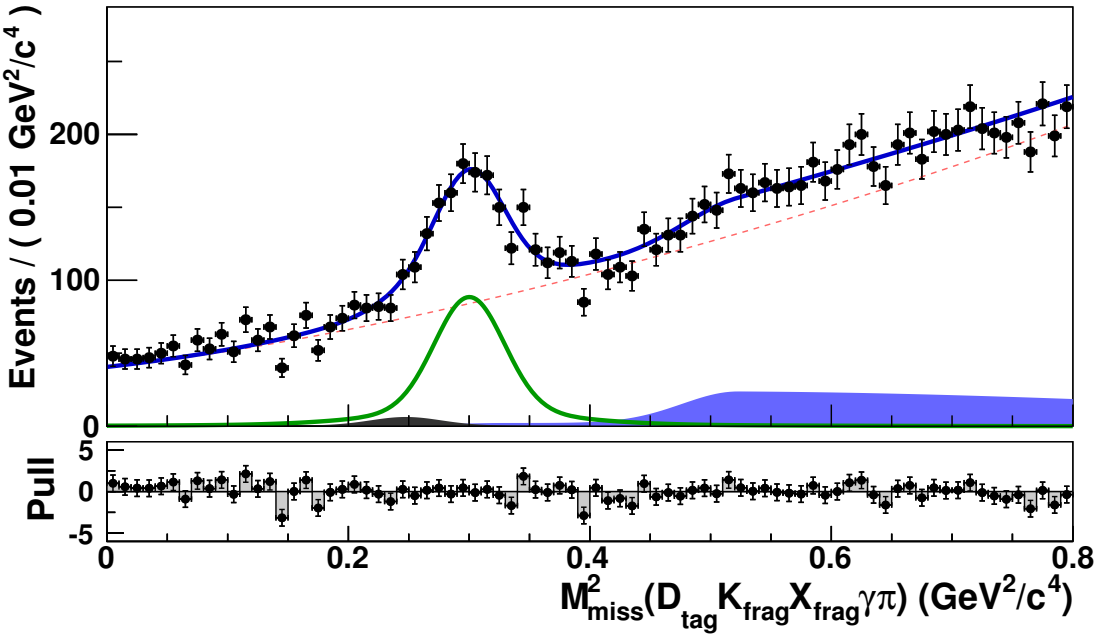

Figure 4. The $M^2_{\rm miss}(D_{\rm tag}K_{\rm frag}X_{\rm frag}\gamma\pi)$ distribution of partially reconstructed $D_s^+ \to \eta\pi^+$ decays within the inclusive D_s^+ sample with superimposed fit results (solid blue line). Solid green line shows the signal contribution, dashed red line contribution of combinatorial background, while the full histograms show the contributions of $D_s^+ \to K^0\pi^+$ (dark gray) or $D_s^+ \to \overline{K}^0K^+$ and $D_s^+ \to \rho^0K^+$ decays (blue).

The signal yield is extracted by performing a binned maximum likelihood fit to the $M^2_{\rm miss}(D_{\rm tag}K_{\rm frag}X_{\rm frag}\gamma\mu)$ distribution. The signal component is parameterized as the sum of three Gaussian functions with a common mean, where all parameters except the mean are fixed to their MC-determined values. As in the case of $D_s^+ \to \eta\pi^+$ decays, the resolution scaling factor of the first and second Gaussians, s, is allowed to float within a Gaussian constraint in the fit, except that the mean and width of the constraint here are set to the value and uncertainty determined in the fits of the $D_s^+ \to \overline{K}^0K^+$ and $D_s^+ \to \eta\pi^+$ candidates ($s = 1.177 \pm 0.049$). The leptonic $D_s^+ \to \tau^+\nu_\tau \to \mu^+\nu_\mu\nu_\tau\overline{\nu}_\tau$ decays produce three neutrinos in the final state and therefore do not peak at $M^2_{\rm miss}(D_{\rm tag}K_{\rm frag}X_{\rm frag}\gamma\mu)$. Their contribution is found to be very well described by an exponential function. In the fit, we include also contributions of hadronic $D_s^+ \to \eta\pi^+$ and $D_s^+ \to \overline{K}^0K^+$ decays where the muon candidate is a misidentified pion or kaon, respectively. The former is parameterized as the sum of two Gaussian functions and the latter as a bifurcated Gaussian function. In both cases, we fix the shape parameters to the MC-determined values. The combinatorial background is parameterized with an exponential function whose shape parameter is fixed to the value determined from the fit to the $M^2_{\rm miss}(D_{\rm tag}K_{\rm frag}X_{\rm frag}\gamma\mu)$ distribution for candidates in the $M_{\rm miss}(D_{\rm tag}K_{\rm frag}X_{\rm frag}\gamma) < 1.95$ GeV/c^2 sideband region. Free parameters of the fits are the yield parameters of all but two spectral components; the $D_s^+ \to \eta\pi^+$ and $D_s^+ \to \overline{K}^0K^+$ yields are constrained to the expected values based on their measured branching fractions and MC-determined efficiencies.

JHEP09(2013)139

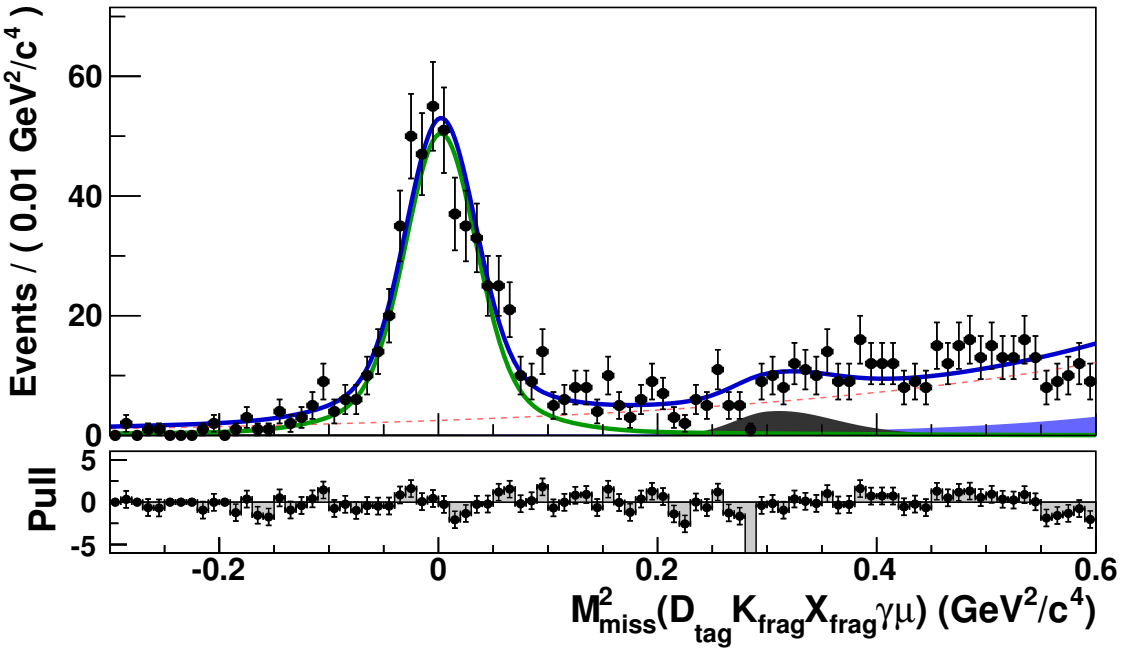

Figure 5. The $M^2_{\rm miss}(D_{\rm tag}K_{\rm frag}X_{\rm frag}\gamma\mu)$ distribution of exclusively reconstructed $D_s^+ \to \mu^+\nu_\mu$ decays within the inclusive D_s^+ sample superimposed fit results (solid blue line). The solid green line shows the contribution of signal, the red dashed line the contribution of combinatorial background, while the contributions of $D_s^+ \to \tau^+\nu_\tau$ and $D_s^+ \to \overline{K}^0K^+$ or $\eta\pi^+$ decays are indicated by the full blue and dark gray histograms, respectively.

The distribution of $M_{\rm miss}(D_{\rm tag}K_{\rm frag}X_{\rm frag}\gamma\mu)$ with superimposed fit is shown in figure 5. The number of reconstructed $D_s^+ \to \mu^+\nu_\mu$ decays is

$$N(D_s^+ \to \mu^+\nu_\mu) = 492 \pm 26, \tag{5.5}$$

where the error is statistical only.

5.5 $D_s^+ \to \tau^+\nu_\tau$

The reconstruction of $D_s^+ \to \tau^+\nu_\tau$ requires one charged track in the rest of the event that is identified as an electron, muon or a pion (denoted as $D_s^+ \to \tau^+(X^+)\nu_\tau$ where $X^+ = e^+,\ \mu^+$ or π^+) indicating the subsequent decay of the τ^+ lepton to $e^+\nu_e\overline{\nu}_\tau$, $\mu^+\nu_\mu\overline{\nu}_\tau$ or $\pi^+\overline{\nu}_\tau$.[5] Due to the multiple neutrinos in the final state, these decays do not peak in the missing-mass-squared distribution:

$$M^2_{\rm miss}(D_{\rm tag}K_{\rm frag}X_{\rm frag}\gamma X) = p^2_{\rm miss}(D_{\rm tag}K_{\rm frag}X_{\rm frag}\gamma X),$$

where the missing four-momentum is given by

$$p_{\rm miss}(D_{\rm tag}K_{\rm frag}X_{\rm frag}\gamma X) = p_{e^+} + p_{e^-} - p_{D_{\rm tag}} - p_{K_{\rm frag}} - p_{X_{\rm frag}} - p_\gamma - p_X.$$

[5]The three decay modes cover almost half of all possible tau decays.

JHEP09(2013)139

The background in the $D_s^+ \to \tau^+(\pi^+)\nu_\tau$ sample is much larger than in the leptonic modes, but is reduced significantly by requiring the magnitude of the missing momentum of the event, $|\vec{p}_{\rm miss}(D_{\rm tag}K_{\rm frag}X_{\rm frag}\gamma\pi)|$, to be larger than 1.2 GeV/c in the laboratory frame. The background in this sample is further reduced by requiring $0.0 < M^2_{\rm miss}(D_{\rm tag}K_{\rm frag}X_{\rm frag}\gamma\pi) < 0.6$ GeV$^2/c^4$.[6] In the case of $D_s^+ \to \tau^+\nu_\tau \to \ell^+\nu_\ell\overline{\nu}_\tau\nu_\tau$ (where $\ell^+ = e^+$ or μ^+), we require $M^2_{\rm miss}(D_{\rm tag}K_{\rm frag}X_{\rm frag}\gamma\ell) > 0.3$ GeV$^2/c^4$ to veto $D_s^+ \to \ell^+\nu_\ell$ decays.

The signal yield of $D_s^+ \to \tau^+\nu_\tau$ decays is extracted from the simultaneous binned maximum likelihood fit to the $E_{\rm ECL}$ distributions of the three tau submodes. The signal decay has either zero or a small value of $E_{\rm ECL}$, while background events tend to have larger values due to the contributions from additional neutral clusters. Signal components include the cross-feed contribution from other τ decays: in the case of leptonic τ decays, the cross-feed contribution is found to be small (around 3% of the signal contribution from leptonic modes) while, in the case of hadronic $\tau^+ \to \pi^+\overline{\nu}_\tau$ decays, a large cross-feed contribution originates from hadronic $\tau^+ \to \rho^+\overline{\nu}_\tau$ decays by missing the neutral pion from the ρ^+ decay (20% of the signal contribution from the pion mode). Backgrounds from several different D_s^+ decays are found to contribute to $D_s^+ \to \tau^+(X^+)\nu_\tau$ samples and are listed in table 3. The peaking background is dominated by D_s^+ decays with K_L^0 in the final state, e.g., $D_s^+ \to \overline{K}^0\ell^+\nu_\ell$ in the case of leptonic tau decays or $D_s^+ \to \overline{K}^0K^+$ in the case of hadronic tau decays. If the K_L^0 deposits little or no energy in the ECL then these decay modes produce an $E_{\rm ECL}$ distribution very similar to the signal. The non-peaking background, dominated by inclusive η decays, is much less problematic since it rises smoothly with increasing $E_{\rm ECL}$. The $E_{\rm ECL}$ distributions of the above categories as well as of the combinatorial background are described with non-parametric histogram PDFs taken from MC samples. In the final fit, four parameters are allowed to vary: the total signal yield summed over three tau decay modes (we fix the relative contribution of the signal from each tau decay mode i to the total signal yield with the ratio of $(\mathcal{B}(\tau \to i)\cdot\varepsilon_i)/\big(\sum_{i=1}^{3}\mathcal{B}(\tau \to i)\cdot\varepsilon_i\big)$ and the yields of combinatorial background in each tau decay mode. The background contributions from D_s^+ decays are fixed to the values given in table 3.

Figure 6 shows the result of the simultaneous fit to the three $E_{\rm ECL}$ distributions for $D_s^+ \to \tau^+(e^+)\nu_\tau$, $D_s^+ \to \tau^+(\mu^+)\nu_\tau$, and $D_s^+ \to \tau^+(\pi^+)\nu_\tau$ decays. The signal yield is

$$N(D_s^+ \to \tau^+\nu_\tau) = 2217 \pm 83, \tag{5.6}$$

where the error is statistical only. As a check, we fit the $E_{\rm ECL}$ distributions while floating the yield of each of the three tau decay modes. The resulting yields are

$$\begin{aligned} N(D_s^+ \to \tau^+(e^+)\nu_\tau) &= 952 \pm 59, \\ N(D_s^+ \to \tau^+(\mu^+)\nu_\tau) &= 758 \pm 48, \\ N(D_s^+ \to \tau^+(\pi^+)\nu_\tau) &= 496 \pm 35, \end{aligned} \tag{5.7}$$

where the errors are statistical only. The sum of individual yields is in good agreement with the total signal yield determined in the simultaneous fit.

[6] Due to the lack of phase space and the fact that $D_s^+ \to \tau^+\nu_\tau \to \pi^+\overline{\nu}_\tau\nu_\tau$ decays have only two neutrinos in the final state, these decays populate a relatively narrow region in $M^2_{\rm miss}(D_{\rm tag}K_{\rm frag}X_{\rm frag}\gamma\pi)$.

JHEP09(2013)139

	Estimated background yields		
Background Source	$\tau^+(e^+)\nu_\tau$	$\tau^+(\mu^+)\nu_\tau$	$\tau^+(\pi^+)\nu_\tau$
$D_s^+ \to \eta\ell^+\nu_\ell$	911.0 ± 102.3	768.7 ± 86.4	–
$D_s^+ \to \eta'\ell^+\nu_\ell$	49.5 ± 12.0	35.1 ± 8.6	–
$D_s^+ \to \phi\ell^+\nu_\ell$	307.8 ± 20.7	188.0 ± 13.3	–
$D_s^+ \to \overline{K}^0\ell^+\nu_\ell$	242.6 ± 66.3	175.7 ± 48.1	–
$D_s^+ \to \overline{K}^{*0}\ell^+\nu_\ell$	26.0 ± 10.5	13.9 ± 5.8	–
$D_s^+ \to K\overline{K}\ell^+\nu_\ell$	59.2 ± 14.5	33.1 ± 8.0	–
$D_s^+ \to \mu^+\nu_\mu$	–	10.0 ± 1.4	26.2 ± 3.7
$D_s^+ \to \overline{K}^0K^+$	18.5 ± 2.5	40.5 ± 4.9	132.3 ± 9.2
$D_s^+ \to \phi\pi^+$	11.2 ± 2.1	14.8 ± 2.5	–
$D_s^+ \to K^{*+}K^0$	32.4 ± 8.3	41.7 ± 10.6	–
$D_s^+ \to \eta\pi^+$	–	–	398.2 ± 24.2
$D_s^+ \to \rho^0K^+$	–	–	185.1 ± 34.9

Table 3. Estimated background yields of various D_s^+ decays contributing to the three $D_s \to \tau^+\nu_\tau$ samples. The uncertainties include the uncertainty of their branching fractions (taken from [2]), the error on the inclusive D_s^+ yield, as well as the uncertainty due to limited MC sample size used to determine the efficiencies and systematic uncertainty related to particle identification.

5.6 $D_s^+ \to e^+\nu_e$

We reconstruct $D_s^+ \to e^+\nu_e$ decays in the same way as $D_s \to \tau^+(e^+)\nu_\tau$ decays, except that we focus on candidates populating the $M^2_{\rm miss}(D_{\rm tag}K_{\rm frag}X_{\rm frag}\gamma e)$ region around zero.[7] To improve the purity, we require that $E_{\rm ECL} < 0.5$ GeV and $p_{\rm miss}(D_{\rm tag}K_{\rm frag}X_{\rm frag}\gamma e) > 0.7$ GeV/c in the laboratory frame. These two requirements reject around 80% of the background candidates while keeping around 75% of the signal candidates in the search window defined as -0.10 GeV$^2/c^4 < M^2_{\rm miss}(D_{\rm tag}K_{\rm frag}X_{\rm frag}\gamma e) < 0.15$ GeV$^2/c^4$. The background in this window is estimated by interpolating the observed yield from missing-mass-squared sidebands: -0.30 GeV$^2/c^4 < M^2_{\rm miss}(D_{\rm tag}K_{\rm frag}X_{\rm frag}\gamma e) < -0.10$ GeV$^2/c^4$ and 0.15 GeV$^2/c^4 < M^2_{\rm miss}(D_{\rm tag}K_{\rm frag}X_{\rm frag}\gamma e) < 0.60$ GeV$^2/c^4$. This is done by performing a binned maximum likelihood fit in these sidebands, using a model consisting of a sum of two exponential functions describing contributions of $D_s^+ \to \tau^+(e^+)\nu_\tau$ decays and combinatorial background. The shape and normalization of the former are fixed to MC-based expectations. Contributions of other D_s^+ decays are found to be negligible. The shape parameter of the combinatorial background is fixed to the value determined in a binned maximum likelihood fit to the $M^2_{\rm miss}(D_{\rm tag}K_{\rm frag}X_{\rm frag}\gamma e)$ distribution of events from $M_{\rm miss}(D_{\rm tag}K_{\rm frag}X_{\rm frag}\gamma)$ sidebands. The normalization of the combinatorial background is a free parameter of the fit. Figure 7 shows the $M^2_{\rm miss}(D_{\rm tag}K_{\rm frag}X_{\rm frag}\gamma e)$ distribution with superimposed fit. We observe

$$n^{e\nu}_{\rm obs} = 8 \tag{5.8}$$

[7] The final states differ only in the number of neutrinos.

JHEP09(2013)139

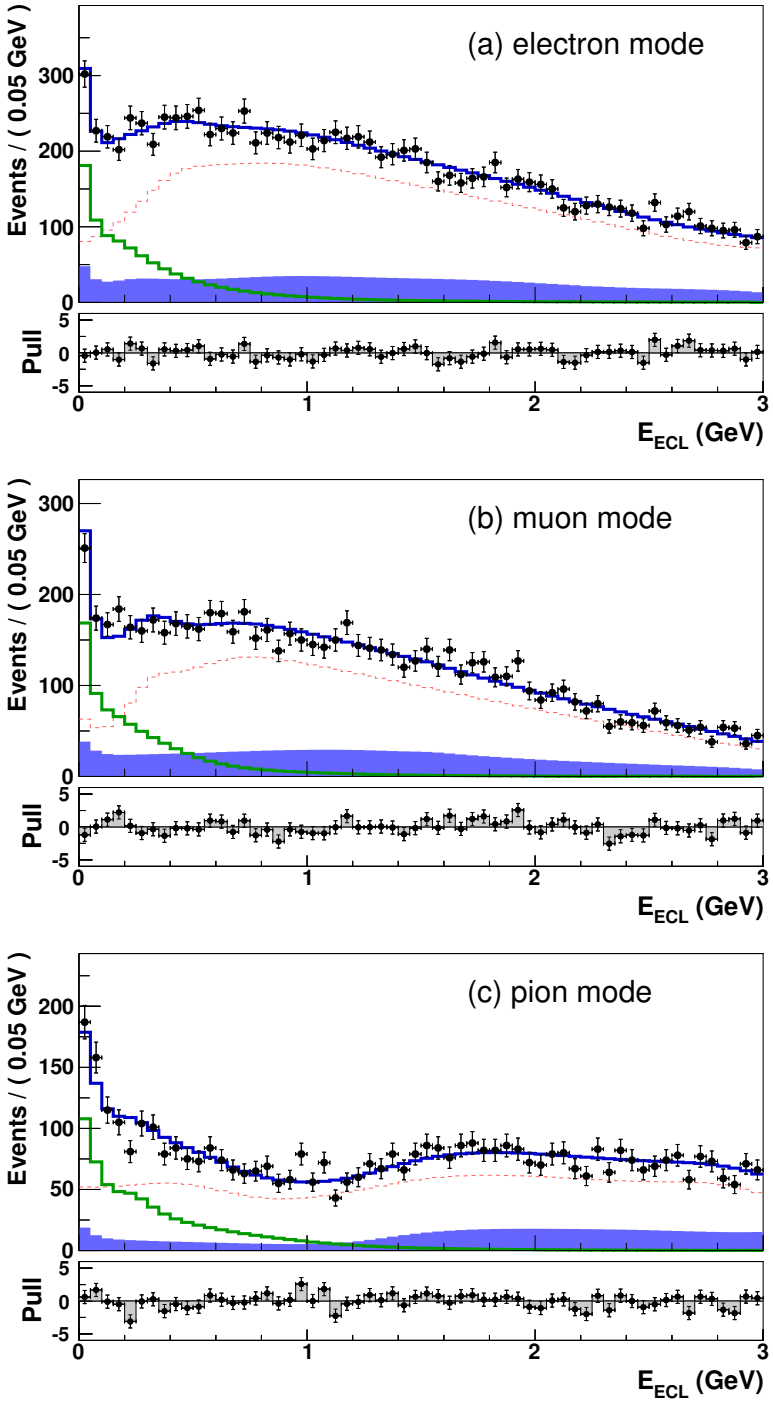

Figure 6. The $E_{\rm ECL}$ distribution of exclusively reconstructed $D_s^+ \to \tau^+(e^+)\nu_\tau$ (a), $D_s^+ \to \tau^+(\mu^+)\nu_\tau$ (b), and $D_s^+ \to \tau^+(\pi^+)\nu_\tau$ (c) decays within the inclusive D_s^+ sample with superimposed fit results. The solid green lines show the contributions of signal and τ cross-feed, the red dashed line the contributions of combinatorial background, while the contributions of background from other $D_s^+ \to f$ decays are shown by the full blue histogram.

JHEP09(2013)139

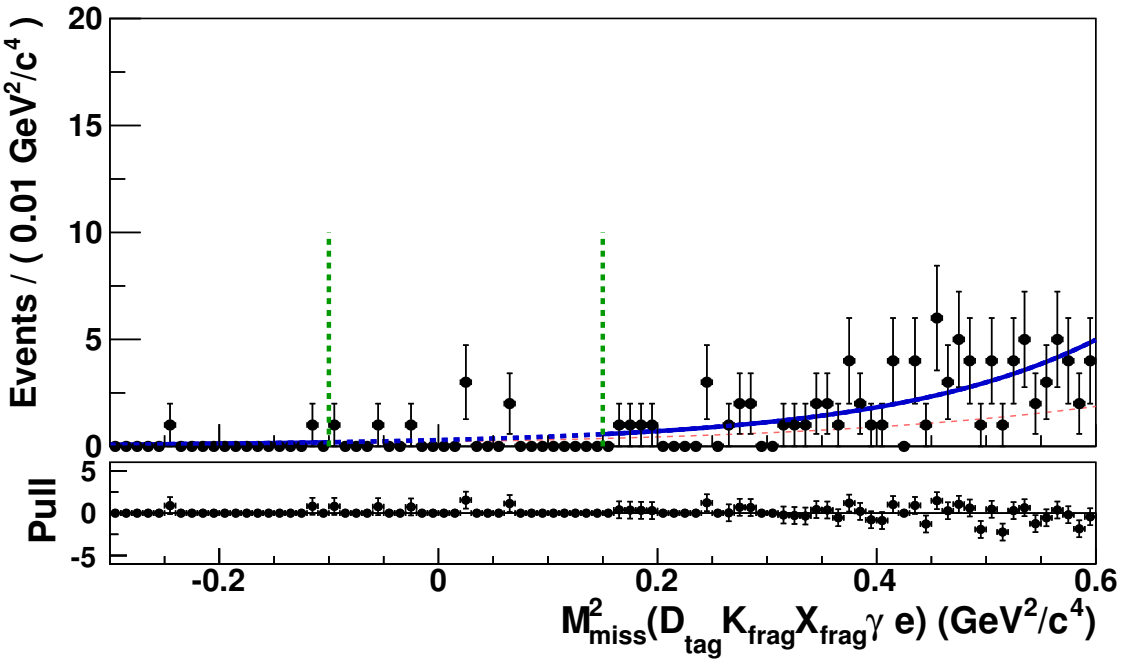

Figure 7. The $M^2_{\rm miss}(D_{\rm tag}K_{\rm frag}X_{\rm frag}\gamma e)$ distribution with superimposed fit results (blue lines). Events populating signal region in $M^2_{\rm miss}(D_{\rm tag}K_{\rm frag}X_{\rm frag}\gamma e)$, denoted with two vertical dashed green lines, are excluded from the fit. The contribution of combinatorial background candidates is indicated with the red dashed line.

in the $M^2_{\rm miss}(D_{\rm tag}K_{\rm frag}X_{\rm frag}\gamma e)$ signal region (denoted by the two vertical lines in figure 7), which is in good agreement with the estimated background

$$b^{e\nu} = 8.7 \pm 0.9(\text{stat.}) \pm 0.8(\text{syst.}), \tag{5.9}$$

where the first error is statistical and the second is systematic. The latter is estimated by varying the yield of $D_s^+ \to \tau^+(e^+)\nu_\tau$ decays and the combinatorial background parameters, changing both shape and normalization, and repeating the fits.

6 Determination of absolute branching fractions

For a given final state f, the absolute branching fraction of the $D_s^+ \to f$ decay is given by

$$\mathcal{B}(D_s^+ \to f) = \frac{N(D_s^+ \to f)}{N^{\rm inc}_{D_s} \cdot f_{\rm bias} \cdot \varepsilon(D_s^+ \to f|\text{incl. } D_s^+)}. \tag{6.1}$$

Here, $N^{\rm inc}_{D_s}$ is the number of inclusively reconstructed D_s^+ mesons (see section 4), $N(D_s^+ \to f)$ is the number of reconstructed $D_s^+ \to f$ decays within the inclusive D_s^+ sample (see section 5), and $\varepsilon(D_s^+ \to f|\text{inc. } D_s^+)$ is the efficiency of reconstructing a $D_s^+ \to f$ decay within the inclusive D_s^+ sample. MC studies show that the D_s^+ inclusive reconstruction efficiency depends on the D_s^+ decay mode and therefore the inclusively reconstructed D_s^+ sample does not represent a truly inclusive sample of D_s^+ mesons. To take this effect

JHEP09(2013)139

D_s^+ decay mode	Signal yield	$f_{\rm bias}\cdot\varepsilon$ [%]	$\mathcal{B}$ [%]
$K^-K^+\pi^+$	4094 ± 123	85.8	$5.06\pm0.15\pm0.21$
$\overline{K}^0K^+$	2018 ± 75	72.5	$2.95\pm0.11\pm0.09$
$\eta\pi^+$	788 ± 59	45.8	$1.82\pm0.14\pm0.07$
$\mu^+\nu_\mu$	492 ± 26	98.2	$0.531\pm0.028\pm0.020$
$\tau^+\nu_\tau$ (e mode)	952 ± 59	18.8	$5.37\pm0.33^{+0.35}_{-0.31}$
$\tau^+\nu_\tau$ (μ mode)	758 ± 48	13.7	$5.86\pm0.37^{+0.34}_{-0.59}$
$\tau^+\nu_\tau$ (π mode)	496 ± 35	8.7	$6.04\pm0.43^{+0.46}_{-0.40}$
$\tau^+\nu_\tau$ (combined)	2217 ± 83	41.2	$5.70\pm0.21^{+0.31}_{-0.30}$

Table 4. Signal yields, tag bias corrected efficiencies and measured branching fractions for all five studied D_s^+ decay modes. The first uncertainty is statistical and the second is systematic. In the case of $D_s^+\to\tau^+\nu_\tau$ decays the efficiencies include the branching fractions of the τ^+ decay modes.

into account, a ratio of D_s^+ inclusive reconstruction efficiency for $D_s^+\to f$ decays, $\varepsilon^{\rm inc}_{D_s\to f}$, and the average D_s^+ inclusive reconstruction efficiency, $\overline{\varepsilon}^{\rm inc}_{D_s}=\sum_i\mathcal{B}(D_s^+\to i)\varepsilon^{\rm inc}_{D_s\to i}$, is included in the denominator of eq. (6.1): $f_{\rm bias}=\varepsilon^{\rm inc}_{D_s\to f}/\overline{\varepsilon}^{\rm inc}_{D_s}$. The ratio $f_{\rm bias}$ is taken from the MC sample.

Measured absolute branching fractions of the $D_s^+\to K^-K^+\pi^+$, $\overline{K}^0K^+$, $\eta\pi^+$, $\mu^+\nu_\mu$, and $\tau^+\nu_\tau$ decays are summarized together with the corresponding signal yields and tag bias corrected efficiencies in table 4.

7 Systematic uncertainties

Systematic uncertainties in the calculation of the branching fractions arise due to imperfect knowledge of the size of the inclusive D_s^+ sample, the reconstruction efficiencies and the modeling of signal and background contributions in the fits from which the signal yields of $D_s^+\to f$ decays are extracted. The estimated systematic uncertainties are itemized in table 5 and described below.

Normalization. The systematic error related to the normalization is assigned to be $\pm2.1\%$ (where statistical and systematic errors given in eq. (4.2) are combined in quadrature) and is common for all studied $D_s^+\to f$ decays.

Tag bias. Possible differences in relative rates of individual D_s^+ decay modes between MC simulation and data that impact the $f_{\rm bias}$ calculation are estimated by studying the distributions of the number of charged particles and π^0's, $N_{\rm ch}+N_{\pi^0}$, produced in D_s^+ decays. We obtain the $N_{\rm ch}+N_{\pi^0}$ data distribution in the following way: first we count the number of remaining charged tracks, $N_{\rm ch}^{\rm reco}$, and π^0 candidates, $N_{\pi^0}^{\rm reco}$, that are not associated to the $D_{\rm tag}K_{\rm frag}X_{\rm frag}\gamma$ candidate; in a second step, we determine, the inclusive D_s^+ yields in bins of the $N_{\rm ch}^{\rm reco}+N_{\pi^0}^{\rm reco}$ by performing fits to the $M_{\rm miss}(D_{\rm tag}K_{\rm frag}X_{\rm frag}\gamma)$ distributions. The obtained distribution of $N_{\rm ch}^{\rm reco}+N_{\pi^0}^{\rm reco}$ is proportional to the true distribution of $N_{\rm ch}+N_{\pi^0}$,

JHEP09(2013)139

Source	$K^-K^+\pi^+$ [%]	$\overline{K}^0K^+$ [%]	$\eta\pi^+$ [%]	$e^+\nu_e$ [%]	$\mu^+\nu_\mu$ [%]	$\tau^+\nu_\tau$ [%]
Normalization	±2.1	±2.1	±2.1	±2.1	±2.1	±2.1
Tag bias	±1.4	±1.4	±1.4	±1.4	±1.4	±1.4
Tracking	±1.1	±0.4	±0.4	±0.4	±0.4	±0.4
Particle ID	±2.6	±0.8	±1.1	±1.9	±2.0	±1.7
Efficiency	±0.7	±0.7	±1.4	±4.3	±1.8	±0.8
Dalitz model	±1.1	–	–	–	–	–
Fit model	±0.8	±0.8	±2.2	–	±0.2	$^{+3.3}_{-2.9}$
D_s^+ background	–	±0.6	±0.7	–	±0.8	±2.8
τ cross-feed	–	–	–	–	–	±0.9
$\mathcal{B}(\tau \to X)$	–	–	–	–	–	±0.2
Total syst.	±4.1	±2.9	±3.9	±5.4	±3.8	$^{+5.4}_{-5.2}$

Table 5. Summary of systematic uncertainties for the branching fraction measurements of D_s^+ decays. The total systematic error is calculated by summing the individual uncertainties in quadrature.

but with a considerable amount of convolution.[8] We obtain the $N_{\rm ch} + N_{\pi^0}$ distribution from the $N_{\rm ch}^{\rm reco} + N_{\pi^0}^{\rm reco}$ distribution using the singular value decomposition algorithm [41]. Finally, we estimate the ratio between the inclusive D_s^+ reconstruction efficiencies in the data and MC samples, $\bar{\varepsilon}_{D_s}^{\rm inc}|_{\rm DATA}/\bar{\varepsilon}_{D_s}^{\rm inc}|_{\rm MC} = 0.9768 \pm 0.0134$, using the unfolded data and MC $N_{\rm ch} + N_{\pi^0}$ distributions and the MC-determined dependence of the inclusive D_s^+ reconstruction efficiency on $N_{\rm ch} + N_{\pi^0}$. The ratio is found to be consistent with unity within the uncertainty. Nevertheless, we correct the measured branching fractions by this factor and assign the error on this ratio as a source of systematic uncertainty ($\pm1.4\%$) that is common for all studied D_s^+ decay modes.

Tracking, particle ID, and efficiency. The systematic errors in the $D_s^+ \to f$ reconstruction efficiencies arise from several sources. First, we assign a 0.35% error per reconstructed charged track in the final state due to the uncertainty on the efficiency of the charged-track reconstruction estimated using partially reconstructed $D^{*+} \to D^0(K_S^0\pi^+\pi^-)\pi^+$ decays. The $e^+e^- \to e^+e^-\ell^+\ell^-$ ($\ell = e$ or μ) and $D^{*+} \to D^0(K^-\pi^+)\pi^+$ samples are used to estimate the lepton, kaon and pion identification corrections and pion (kaon) to lepton misidentification probabilities. Finally, we include statistical uncertainties of the MC-determined efficiencies $f_{\rm bias} \cdot \varepsilon(D_s^+ \to f|\text{inc. } D_s^+)$ as a source of systematic error. Since the branching fractions are determined relative to the number of inclusively reconstructed D_s^+ mesons, the systematic uncertainties in the reconstruction of the inclusive D_s^+ cancel.

[8] E.g., a D_s^+ daughter particle might not be reconstructed or a fake charged track or π^0 candidate may be counted.

JHEP09(2013)139

Dalitz model. In the case of $D_s^+ \to K^-K^+\pi^+$ decays, the reconstruction efficiency varies weakly across the $K^-K^+\pi^-$ Dalitz distribution. In calculating $\mathcal{B}(D_s^+ \to K^-K^+\pi^+)$, we use the Dalitz-plot-integrated MC efficiency. The decay amplitude in the MC is simply the incoherent sum of all known resonant two-body contributions ($\phi\pi^+$, $\overline{K}^{*0}K^+$, $f_0(980)\pi^+$ and others). We use a dedicated MC in which the $D_s^+ \to K^-K^+\pi^+$ decay dynamics are simulated according to results of the Dalitz plot analysis performed by the CLEO collaboration [42]. The ratio of efficiencies from both samples is found to be consistent with unity within the uncertainty ($\pm 1.1\%$) which is conservatively assigned as a source of systematic error.

Fit model. The systematic error due to limited statistics of the MC sample used to construct the histogram PDFs is evaluated by varying repeatedly the contents of all bins of all histogram PDFs within their statistical uncertainties and refitting. The RMS of the distribution of fit results is assigned as a systematic uncertainty due to the fit model. To estimate the systematic error due to the possible signal $E_{\rm ECL}$ shape difference between MC and data, we use the ratio of data to MC for the $E_{\rm ECL}$ histograms of the background-subtracted $D_s^+ \to K^-K^+\pi^+$ and $D_s^+ \to \overline{K}^0K^+$ samples to modify the signal PDF and repeat the fit. In a similar way, we estimate the systematic error due to the possible $E_{\rm ECL}$ shape difference of combinatorial background in MC and data by using the ratio of $E_{\rm ECL}$ histograms of $D_s^+ \to \tau^+\nu_\tau$ candidates populating the $M_{\rm miss}(D_{\rm tag}K_{\rm frag}X_{\rm frag}\gamma)$ sidebands and modifying accordingly the combinatorial $E_{\rm ECL}$ PDF. For $D_s^+ \to \mu^+\nu_\mu$, $D_s^+ \to \overline{K}^0K^+$, and $D_s^+ \to \eta\pi^+$ decays, we vary the values of all fixed parameters within their uncertainties (taking correlations into account) and assign the differences with respect to the nominal fits as the fit model systematic uncertainty. In the case of $D_s^+ \to K^-K^+\pi^+$, the fits are repeated by changing $\sigma_{\rm cal}^{\rm excl}$ within its uncertainty to assess this source of systematic error.

D_s^+ background. In the fits, we fix the contributions of certain background D_s^+ decays to the expectations based on their measured branching fractions. We estimate the systematic error related to this by changing these branching fractions by their experimental errors [2]. In the case of $D_s^+ \to \tau^+(e^+)\nu_\tau$ and $D_s^+ \to \tau^+(\mu^+)\nu_\tau$ decays, the systematic uncertainty from this source originates mainly from $D_s^+ \to \overline{K}^0\ell\nu$ decays; in the case of $D_s^+ \to \tau^+(\pi^+)\nu_\tau$, from $D_s^+ \to \eta\pi^+$ and $D_s^+ \to \rho K^+$ decays.

τ cross-feed. In the nominal fit to the $E_{\rm ECL}$ distribution of reconstructed $D_s^+ \to \tau^+\nu_\tau$ decays, we fix the cross-feed contributions relative to the signal contributions. We vary the ratios of cross-feed candidates within their uncertainties, repeat the fits, and take the differences from the nominal fits as the systematic uncertainty.

$\mathcal{B}(\tau \to X)$. We include the uncertainties of the branching fractions of τ^+ decays to $e^+\nu_e\overline{\nu}_\tau$, $\mu^+\nu_\mu\overline{\nu}_\tau$ and $\pi^+\overline{\nu}_\tau$ [2] as the systematic errors on $\mathcal{B}(D_s^+ \to \tau^+\nu_\tau)$.

JHEP09(2013)139

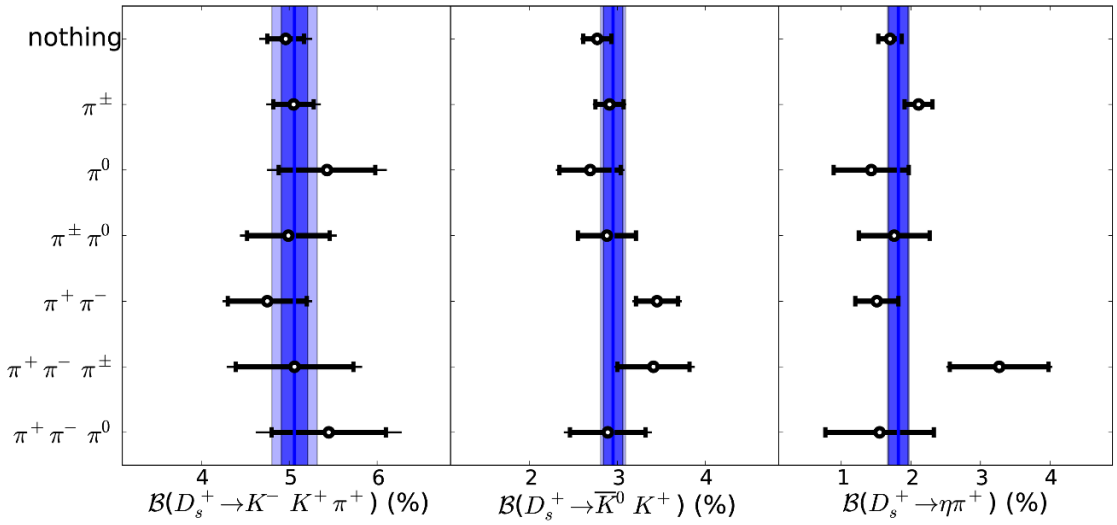

Figure 8. The measured $\mathcal{B}(D_s^+ \to K^-K^+\pi^+)$ (left), $\mathcal{B}(D_s^+ \to \overline{K}^0K^+)$ (middle), and $\mathcal{B}(D_s^+ \to \eta\pi^+)$ (right) for each $X_{\rm frag}$ mode. The measured branching fractions when all $X_{\rm frag}$ modes are combined are indicated with vertical blue lines with statistical and total errors indicated as inner (dark blue) and outer (light blue) bands.

8 Results

8.1 Branching fractions

The signal yields of reconstructed $D_s^+ \to K^-K^+\pi^+$, $\overline{K}^0K^+$, $\eta\pi^+$, $\mu^+\nu_\mu$, and $\tau^+\nu_\tau$ decays within the inclusive D_s^+ sample are used to determine their absolute branching fractions (see also table 4). We measure the branching fractions of hadronic D_s^+ decays to be

$$\mathcal{B}(D_s^+ \to K^-K^+\pi^+) = (5.06 \pm 0.15(\text{stat.}) \pm 0.21(\text{syst.})) \times 10^{-2}, \tag{8.1}$$
$$\mathcal{B}(D_s^+ \to \overline{K}^0K^+) = (2.95 \pm 0.11(\text{stat.}) \pm 0.09(\text{syst.})) \times 10^{-2}, \tag{8.2}$$
$$\mathcal{B}(D_s^+ \to \eta\pi^+) = (1.82 \pm 0.14(\text{stat.}) \pm 0.07(\text{syst.})) \times 10^{-2}. \tag{8.3}$$

As a check, we determine the branching fractions of hadronic D_s^+ decays for each $X_{\rm frag}$ mode separately. Figure 8 shows the measured branching fractions of the three hadronic decay modes, subdivided by $X_{\rm frag}$ mode. They are found to be in good agreement within uncertainties.

We measure the branching fractions of leptonic D_s^+ decays to be

$$\mathcal{B}(D_s^+ \to \mu^+\nu_\mu) = (5.31 \pm 0.28(\text{stat.}) \pm 0.20(\text{syst.})) \times 10^{-3}, \tag{8.4}$$
$$\mathcal{B}(D_s^+ \to \tau^+\nu_\tau) = (5.70 \pm 0.21(\text{stat.})^{+0.31}_{-0.30}(\text{syst.})) \times 10^{-2}, \tag{8.5}$$

where the first uncertainties are statistical and second systematic. The measured value of $\mathcal{B}(D_s^+ \to \mu^+\nu_\mu)$ is consistent with and represents a significant improvement over the previously measured value of $\mathcal{B}(D_s^+ \to \mu^+\nu_\mu) = (6.44 \pm 0.76(\text{stat.}) \pm 0.57(\text{syst.})) \times 10^{-3}$ by Belle [14]. Table 4 gives also the branching fractions of $D_s^+ \to \tau^+\nu_\tau$ decays as determined

JHEP09(2013)139

for individual τ^+ decay modes. They are in good agreement within statistical uncertainties. As a test of lepton flavor universality, we determine the ratio of D_s^+ leptonic decays to tau and muon to be

$$R_{\tau/\mu}^{D_s} = 10.73 \pm 0.69(\text{stat.})^{+0.56}_{-0.53}(\text{syst.}), \tag{8.6}$$

where we have taken into account that the common systematics between the two decay modes cancel in the ratio. The measured $R_{\tau/\mu}^{D_s}$ is in agreement with the SM value of 9.762 ± 0.031.

We find no evidence for $D_s^+ \to e^+\nu_e$ decays and set an upper limit on $\mathcal{B}(D_s^+ \to e^+\nu_e)$ using the modified frequentist approach (or CL_s method) [43, 44]. We construct test statistics from pseudo-experiments according to the signal plus background and background-only hypotheses [45]. For each pseudo-experiment, a likelihood ratio is computed depending on the expected number of signal events for a given value of $\mathcal{B}(D_s^+ \to e^+\nu_e)$ (according to eq. (6.1)),

$$\begin{aligned} s^{e\nu} &= N_{\text{incl.}}^{D_s} \cdot f_{\text{bias}} \cdot \varepsilon(D_s^+ \to e^+\nu|\text{incl. } D_s^+) \cdot \mathcal{B}(D_s^+ \to e^+\nu_e) \\ &= (59370 \pm 3150(\text{stat.} + \text{syst.})) \cdot \mathcal{B}(D_s^+ \to e^+\nu_e), \end{aligned} \tag{8.7}$$

the expected number of background events, $b^{e\nu}$ (see eq. (5.9)), and the observed number of events, $n_{\text{obs}}^{e\nu}$ (see eq. (5.8)). The CL_s is defined as the ratio of confidence levels, $\text{CL}_{\text{s+b}}/\text{CL}_\text{b}$, where the $\text{CL}_{\text{s+b}}$ and CL_b are the probabilities for signal-plus-background or background-only generated pseudo-experiments, respectively, to have a test-statistic value larger than or equal to that observed in the data. The observed distribution of CL_s as a function of branching fraction of $D_s^+ \to e^+\nu_e$ decays is shown in figure 9. The upper limits on $\mathcal{B}(D_s^+ \to e^+\nu_e)$ at 95 (90)% confidence level (C.L.), which corresponds to $\text{CL}_\text{s} = 0.05$ (0.1), are

$$\mathcal{B}(D_s^+ \to e^+\nu_e) < 1.0\ (0.83) \times 10^{-4} \text{ at } 95\ (90)\% \text{ C.L.} \tag{8.8}$$

The systematic uncertainties of $s^{e\nu}$ and $b^{e\nu}$ are included in the CL_s method using the techniques described in refs. [43, 44]. The sources of systematic uncertainties that are considered in the evaluation of $s^{e\nu}$ are listed in table 5.

8.2 Extraction of the D_s^+ meson decay constant

The value of f_{D_s} is determined from the measured branching fractions of leptonic D_s^+ decays. Inverting eq. (1.1) yields

$$f_{D_s} = \frac{1}{G_F m_\ell \left(1 - \frac{m_\ell^2}{m_{D_s}^2}\right) |V_{cs}|} \sqrt{\frac{8\pi \mathcal{B}(D_s^+ \to \ell^+\nu_\ell)}{m_{D_s} \tau_{D_s}}}.$$

The external inputs necessary in the extraction of f_{D_s} from the measured branching fractions are given in table 6. The CKM matrix element $|V_{cs}|$ is obtained from the well-measured $|V_{ud}| = 0.97425 \pm 0.00022$ and $|V_{cb}| = (40.9 \pm 1.1) \times 10^{-3}$ [2] by using the relation $|V_{cs}| = |V_{ud}| - |V_{cb}|^2/2$, following the prescription given in the section *Decay constants of charged pseudoscalar mesons* in ref. [2]. All but one of the external inputs are very

JHEP09(2013)139

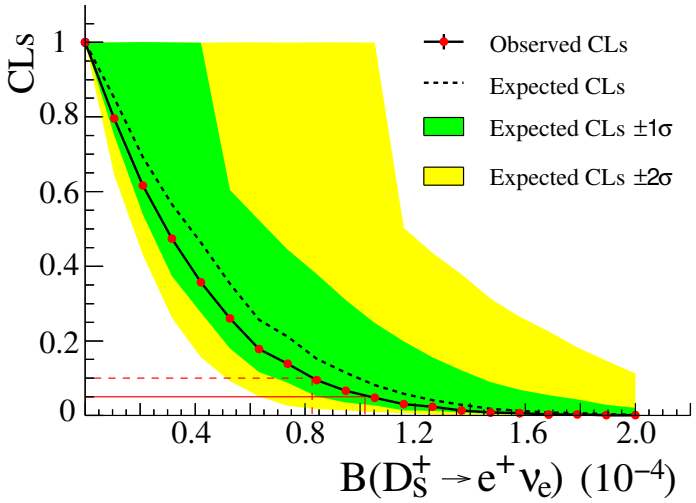

Figure 9. Observed (solid curve) and expected (dashed curve) CL_s values as a function of $\mathcal{B}(D_s^+ \to e^+\nu_e)$. The green (yellow) shaded area contains the $\pm 1\ \sigma$ ($\pm 2\ \sigma$) interval of possible results compatible with the expected value if only background is observed. The upper limits at the 90% (95%) C.L. are indicated by the dashed (solid) line.

Quantity	Value
m_{D_s}	1.96849(32) GeV
m_τ	1.77682(16) GeV
m_μ	0.1056583715(35) GeV
τ_{D_s}	0.500(7) ps
G_F	$1.16637(1) \times 10^{-5}$ GeV^{-2}
$\lvert V_{cs}\rvert$	0.97341(22)

Table 6. Numerical values of external parameters used in extraction of f_{D_s}. All values are taken from ref. [2] except for $|V_{cs}|$ where we follow the prescription given in the section *Decay constants of charged pseudoscalar mesons* of ref. [2].

precisely measured and do not introduce additional uncertainties; the exception is the D_s^+ lifetime, τ_{D_s}, which introduces an 0.70% relative uncertainty. Table 7 summarizes the obtained values of f_{D_s} using the $D_s^+ \to \mu^+\nu_\mu$ and $D_s^+ \to \tau^+\nu_\tau$ decays. The error-weighted average is

$$f_{D_s} = (255.5 \pm 4.2(\text{stat.}) \pm 4.8(\text{syst.}) \pm 1.8(\tau_{D_s}))\ \text{MeV},$$

where the correlation of the systematic uncertainties between the $\mu^+\nu_\mu$ and $\tau^+\nu_\tau$ have been taken into account. This is the most precise measurement of f_{D_s} to date.

9 Conclusions

In conclusion, we measure the absolute branching fractions of hadronic decays to $K^-K^+\pi^+$, $\overline{K}^0K^+$, and $\eta\pi^+$, and of leptonic D_s^+ decays to $\mu^+\nu_\mu$ and $\tau^+\nu_\tau$ using the large data sample collected by the Belle experiment at the KEKB collider. The branching fractions of

JHEP09(2013)139

$D_s^+ \to \ell^+\nu_\ell$	f_{D_s} [MeV]
$\mu^+\nu_\mu$	$249.8 \pm 6.6(\text{stat.}) \pm 4.7(\text{syst.}) \pm 1.7(\tau_{D_s})$
$\tau^+\nu_\tau$	$261.9 \pm 4.9(\text{stat.}) \pm 7.0(\text{syst.}) \pm 1.8(\tau_{D_s})$
Combination	$255.5 \pm 4.2(\text{stat.}) \pm 4.8(\text{syst.}) \pm 1.8(\tau_{D_s})$

Table 7. Measured values of f_{D_s} in $\mu^+\nu_\mu$ and $\tau^+\nu_\tau$ decay modes and their combination.

hadronic D_s^+ decays are in agreement with the measurements performed by CLEO [27, 28]. The measurements of branching fractions of leptonic D_s^+ decays are consistent with the previous measurements performed by the CLEO and BaBar collaborations [11–13, 15]. From the measured branching fractions of leptonic D_s^+ decays, we determine the D_s^+ meson decay constant, $f_{D_s} = (255.5 \pm 4.2(\text{stat.}) \pm 4.8(\text{syst.}) \pm 1.8(\tau_{\text{D}_\text{s}}))$ MeV, which represents the single most precise measurement to date and is found to be in agreement with the most precise lattice QCD calculation [16]. We find no evidence for $D_s^+ \to e^+\nu_e$ decays and we set the most stringent upper limit of $\mathcal{B}(D_s^+ \to e^+\nu_e) < 1.0\ (0.83) \times 10^{-4}$ at 95 (90)% C.L.

Acknowledgments

We thank the KEKB group for the excellent operation of the accelerator; the KEK cryogenics group for the efficient operation of the solenoid; and the KEK computer group, the National Institute of Informatics, and the PNNL/EMSL computing group for valuable computing and SINET4 network support. We acknowledge support from the Ministry of Education, Culture, Sports, Science, and Technology (MEXT) of Japan, the Japan Society for the Promotion of Science (JSPS), and the Tau-Lepton Physics Research Center of Nagoya University; the Australian Research Council and the Australian Department of Industry, Innovation, Science and Research; Austrian Science Fund under Grant No. P 22742-N16; the National Natural Science Foundation of China under contract No. 10575109, 10775142, 10875115 and 10825524; the Ministry of Education, Youth and Sports of the Czech Republic under contract No. MSM0021620859; the Carl Zeiss Foundation, the Deutsche Forschungsgemeinschaft and the VolkswagenStiftung; the Department of Science and Technology of India; the Istituto Nazionale di Fisica Nucleare of Italy; The BK21 and WCU program of the Ministry Education Science and Technology, National Research Foundation of Korea Grant No. 2010-0021174, 2011-0029457, 2012-0008143, 2012R1A1A2008330, BRL program under NRF Grant No. KRF-2011-0020333, and GSDC of the Korea Institute of Science and Technology Information; the Polish Ministry of Science and Higher Education and the National Science Center; the Ministry of Education and Science of the Russian Federation and the Russian Federal Agency for Atomic Energy; the Slovenian Research Agency; the Basque Foundation for Science (IKERBASQUE) and the UPV/EHU under program UFI 11/55; the Swiss National Science Foundation; the National Science Council and the Ministry of Education of Taiwan; and the U.S. Department of Energy and the National Science Foundation. This work is supported by a Grant-in-Aid from MEXT for Science Research in a Priority Area ("New Development of Flavor Physics"), and from JSPS for Creative Scientific Research ("Evolution of Tau-lepton Physics").

JHEP09(2013)139

References

[1] Belle collaboration, J. Brodzicka et al., *Physics Achievements from the Belle Experiment*, *Prog. Theor. Exp. Phys.* **2012** (2012) 04D001 [arXiv:1212.5342] [INSPIRE].

[2] Particle Data Group collaboration, J. Beringer et al., *Review of Particle Physics (RPP)*, *Phys. Rev.* **D 86** (2012) 010001 [INSPIRE].

[3] Belle collaboration, I. Adachi et al., *Measurement of $B^- \to \tau^- \bar{\nu}_\tau$ with a Hadronic Tagging Method Using the Full Data Sample of Belle*, *Phys. Rev. Lett.* **110** (2013) 131801 [arXiv:1208.4678] [INSPIRE].

[4] Belle collaboration, K. Hara et al., *Evidence for $B^- \to \tau^- \bar{\nu}$ with a Semileptonic Tagging Method*, *Phys. Rev.* **D 82** (2010) 071101 [arXiv:1006.4201] [INSPIRE].

[5] LHCb collaboration, *First Evidence for the Decay $B_s^0 \to \mu^+ \mu^-$*, *Phys. Rev. Lett.* **110** (2013) 021801 [arXiv:1211.2674] [INSPIRE].

[6] A. Akeroyd and C.H. Chen, *Effect of $H^\pm$ on $B^\pm \to \tau^\pm \nu_\tau$ and $D_s^\pm \to \mu^\pm \nu_\mu$, $\tau^\pm \nu_\tau$*, *Phys. Rev.* **D 75** (2007) 075004 [hep-ph/0701078] [INSPIRE].

[7] A. Akeroyd and F. Mahmoudi, *Constraints on charged Higgs bosons from $D_s^\pm \to \mu^\pm \nu$ and $D_s^\pm \to \tau^\pm \nu$*, *JHEP* **04** (2009) 121 [arXiv:0902.2393] [INSPIRE].

[8] J. Barranco, D. Delepine, V.G. Macias and L. Lopez-Lozano, *Constraining New Physics with D meson decays*, arXiv:1303.3896 [INSPIRE].

[9] A. Crivellin, A. Kokulu and C. Greub, *Flavor-phenomenology of two-Higgs-doublet models with generic Yukawa structure*, *Phys. Rev.* **D 87** (2013) 094031 [arXiv:1303.5877] [INSPIRE].

[10] A. Filipuzzi, J. Portoles and M. Gonzalez-Alonso, $U(2)^5$ *flavor symmetry and lepton universality violation in $W \to \tau \nu_\tau$*, *Phys. Rev.* **D 85** (2012) 116010 [arXiv:1203.2092] [INSPIRE].

[11] CLEO collaboration, J. Alexander et al., *Measurement of $BD_s^+ \to \ell^+ \nu$ and the Decay Constant $f D_s^+$ From 600 /pb^{-1} of $e^\pm$ Annihilation Data Near 4170 MeV*, *Phys. Rev.* **D 79** (2009) 052001 [arXiv:0901.1216] [INSPIRE].

[12] CLEO collaboration, P. Naik et al., *Measurement of the Pseudoscalar Decay Constant f_{D_s} Using $D_s^+ \to \tau^+ \nu$, $\tau^+ \to \rho^+ \overline{\nu}$ Decays*, *Phys. Rev.* **D 80** (2009) 112004 [arXiv:0910.3602] [INSPIRE].

[13] CLEO collaboration, P. Onyisi et al., *Improved Measurement of Absolute Branching Fraction of $D_s^+ \to \tau^+ \nu_\tau$*, *Phys. Rev.* **D 79** (2009) 052002 [arXiv:0901.1147] [INSPIRE].

[14] Belle collaboration, L. Widhalm et al., *Measurement of $B(D_s^+ \to \mu^+ \nu)$*, *Phys. Rev. Lett.* **100** (2008) 241801 [arXiv:0709.1340] [INSPIRE].

[15] BaBar collaboration, P. del Amo Sanchez et al., *Measurement of the Absolute Branching Fractions for $D_s^- \to \ell^- \bar{\nu}_\ell$ and Extraction of the Decay Constant f_{D_s}*, *Phys. Rev.* **D 82** (2010) 091103 [arXiv:1008.4080] [INSPIRE].

JHEP09(2013)139

[16] C. Davies et al., *Update: Precision D_s decay constant from full lattice QCD using very fine lattices*, *Phys. Rev.* **D 82** (2010) 114504 [arXiv:1008.4018] [INSPIRE].

[17] FERMILAB LATTICE COLLABORATION, MILC collaboration, A. Bazavov et al., *B- and D-meson decay constants from three-flavor lattice QCD*, *Phys. Rev.* **D 85** (2012) 114506 [arXiv:1112.3051] [INSPIRE].

[18] D. Becirevic, B. Blossier, A. Gerardin, A. Le Yaouanc and F. Sanfilippo, *On the significance of B-decays to radially excited D*, *Nucl. Phys.* **B 872** (2013) 313 [arXiv:1301.7336] [INSPIRE].

[19] ETM collaboration, B. Blossier et al., *Pseudoscalar decay constants of kaon and D-mesons from $N_f = 2$ twisted mass Lattice QCD*, *JHEP* **07** (2009) 043 [arXiv:0904.0954] [INSPIRE].

[20] J. Bordes, J. Penarrocha and K. Schilcher, *D and D_S decay constants from QCD duality at three loops*, *JHEP* **11** (2005) 014 [hep-ph/0507241] [INSPIRE].

[21] W. Lucha, D. Melikhov and S. Simula, *OPE, charm-quark mass and decay constants of D and D_s mesons from QCD sum rules*, *Phys. Lett.* **B 701** (2011) 82 [arXiv:1101.5986] [INSPIRE].

[22] A. Badalian, B. Bakker and Y. Simonov, *Decay constants of the heavy-light mesons from the field correlator method*, *Phys. Rev.* **D 75** (2007) 116001 [hep-ph/0702157] [INSPIRE].

[23] C.-W. Hwang, SU(3) *symmetry breaking in decay constants and electromagnetic properties of pseudoscalar heavy mesons*, *Phys. Rev.* **D 81** (2010) 054022 [arXiv:0910.0145] [INSPIRE].

[24] R. Fleischer, N. Serra and N. Tuning, *A New Strategy for B_s Branching Ratio Measurements and the Search for New Physics in $B_s^0 \to mu^+mu^-$*, *Phys. Rev.* **D 82** (2010) 034038 [arXiv:1004.3982] [INSPIRE].

[25] LHCB collaboration, *Measurement of b-hadron production fractions in* 7 TeVpp *collisions*, *Phys. Rev.* **D 85** (2012) 032008 [arXiv:1111.2357] [INSPIRE].

[26] LHCB collaboration, *Measurement of the fragmentation fraction ratio f_s/f_d and its dependence on B meson kinematics*, *JHEP* **04** (2013) 001 [arXiv:1301.5286] [INSPIRE].

[27] CLEO collaboration, J. Alexander et al., *Absolute Measurement of Hadronic Branching Fractions of the D_s^+ Meson*, *Phys. Rev. Lett.* **100** (2008) 161804 [arXiv:0801.0680] [INSPIRE].

[28] CLEO collaboration, P. Onyisi et al., *Improved Measurement of Absolute Hadronic Branching Fractions of the D_s^+ Meson*, *Phys. Rev. D 88,* **032009** (2013) [arXiv:1306.5363] [INSPIRE].

[29] S. Kurokawa, *Overview of the KEKB accelerators*, *Nucl. Instrum. Meth.* **A 499** (2003) 1 [INSPIRE].

[30] T. Abe et al., *Achievements of KEKB*, *Prog. Theor. Exp. Phys.* **2013** (2013) 03A001.

[31] BELLE collaboration, A. Abashian et al., *The Belle Detector*, *Nucl. Instrum. Meth.* **A 479** (2002) 117 [INSPIRE].

[32] D. Lange, *The EvtGen particle decay simulation package*, *Nucl. Instrum. Meth.* **A 462** (2001) 152 [INSPIRE].

[33] T. Sjöstrand, *High-energy physics event generation with PYTHIA 5.7 and JETSET 7.4*, *Comput. Phys. Commun.* **82** (1994) 74 [INSPIRE].

[34] R. Brun, F. Bruyant, M. Maire, A. McPherson and P. Zanarini, *GEANT3* (1987).

JHEP09(2013)139

[35] E. Barberio and Z. Was, *PHOTOS: A Universal Monte Carlo for QED radiative corrections. Version 2.0*, *Comput. Phys. Commun.* **79** (1994) 291 [INSPIRE].

[36] BELLE collaboration, L. Widhalm et al., *Measurement of $D^0 \to \pi\ell\nu$ ($K\ell\nu$) Form Factors and Absolute Branching Fractions*, *Phys. Rev. Lett.* **97** (2006) 061804 [hep-ex/0604049] [INSPIRE].

[37] M. Feindt and U. Kerzel, *The NeuroBayes neural network package*, *Nucl. Instrum. Meth.* **A 559** (2006) 190 [INSPIRE].

[38] M. Pivk and F.R. Le Diberder, *${}_S\mathcal{P}lot$: A Statistical tool to unfold data distributions*, *Nucl. Instrum. Meth.* **A 555** (2005) 356 [physics/0402083] [INSPIRE].

[39] V. Blobel, Smoothing of Poisson distributed data, http://www.desy.de/~blobel/splft.f.

[40] CLEO collaboration, H. Mendez et al., *Measurements of D Meson Decays to Two Pseudoscalar Mesons*, *Phys. Rev.* **D 81** (2010) 052013 [arXiv:0906.3198] [INSPIRE].

[41] A. Höcker and V. Kartvelishvili, *SVD approach to data unfolding*, *Nucl. Instrum. Meth.* **A 372** (1996) 469 [hep-ph/9509307] [INSPIRE].

[42] CLEO collaboration, R. Mitchell et al., *Dalitz Plot Analysis of $D_s^+ \to K^+K^-\pi^+$*, *Phys. Rev.* **D 79** (2009) 072008 [arXiv:0903.1301] [INSPIRE].

[43] T. Junk, *Confidence level computation for combining searches with small statistics*, *Nucl. Instrum. Meth.* **A 434** (1999) 435 [hep-ex/9902006] [INSPIRE].

[44] A.L. Read, *Presentation of search results: The CL_s technique*, *J. Phys.* **G 28** (2002) 2693 [INSPIRE].

[45] L. Moneta et al., *The RooStats Project*, PoS(ACAT2010)057 [arXiv:1009.1003] [INSPIRE].

JHEP09(2013)139